

Diffusion Path Samplers via Sequential Monte Carlo

James Matthew Young^{*†}, Paula Cordero-Encinar[†],
 Sebastian Reich[‡], Andrew Duncan[†], and Ö. Deniz Akyildiz[†]

[†]Department of Mathematics, Imperial College London, UK

[‡]Institut für Mathematik, Universität Potsdam, Germany

January 30, 2026

Abstract

We develop a diffusion-based sampler for target distributions known up to a normalising constant. To this end, we rely on the well-known diffusion path that smoothly interpolates between a (simple) base distribution and the target distribution, widely used in diffusion models. Our approach is based on a practical implementation of *diffusion-annealed Langevin Monte Carlo*, which approximates the diffusion path with convergence guarantees. We tackle the score estimation problem by developing an efficient sequential Monte Carlo sampler that evolves auxiliary variables from conditional distributions along the path, which provides principled score estimates for time-varying distributions. We further develop novel control variate schedules that minimise the variance of these score estimates. Finally, we provide theoretical guarantees and empirically demonstrate the effectiveness of our method on several synthetic and real-world datasets.

1 Introduction

Sampling from a target distribution $\pi \propto e^{-V_\pi}$ known up to a normalising constant is a fundamental problem in many fields of science. It underpins Bayesian inference [Gelman et al., 1995], machine learning [Bishop and Nasrabadi, 2006], statistical physics [Newman and Barkema, 1999], finance [Glasserman, 2004], computational biology [Wilkinson, 2018], and many others. Sampling directly from complex targets is a notoriously difficult task. A standard way to avoid this issue is to introduce an auxiliary path of distributions bridging an easy-to-sample-from base density and the target density [Neal, 2001, Del Moral et al., 2006]. This allows the sampler to gradually adapt to the complexity of the target distribution instead of tackling it directly. A popular idea in this line of work has been to consider the so-called *geometric path*, which is shown to introduce spurious modes along the way [Chehab et al., 2025, Cordero-Encinar et al., 2025a] that can severely hinder the efficiency of the sampling procedure.

In this work, we instead focus on a powerful alternative, the *diffusion path*, which has recently gained significant attention in the generative modelling literature [Sohl-Dickstein et al., 2015, Ho et al., 2020, Song et al., 2021]. As opposed to the geometric path, the diffusion path remains well behaved: under mild assumptions, it admits uniformly bounded functional inequalities and finite action [Cordero-Encinar et al., 2025a]. Geometric paths, on the other hand, can induce multimodality and degradation of log-Sobolev constants, leading to inferior sampling performance [Chehab et al., 2025]. These regularity properties, combined with the performance of diffusion models in high-dimensional generative tasks, make the diffusion path an appealing choice for sampling and have motivated a number of recent contributions (see Section 2.2 for a detailed discussion of recent works and comparisons).

In this work, we expand this area by developing a diffusion-annealed Langevin sampler based on sequential Monte Carlo (SMC). Specifically, our contributions are:

*Corresponding author: mmy20@ic.ac.uk

- We develop a sampler based on an implementation of diffusion-annealed Langevin dynamics [Cordero-Encinar et al., 2025a] for sampling along diffusion paths. Notably, to estimate time-varying scores, we build SMC samplers [Del Moral et al., 2006] that evolve auxiliary variables in a non-equilibrium manner, leading to a highly parallelisable and efficient sampler.
- We introduce novel control variate schedules for minimising the variance of score estimates, describing their optimum under certain regimes and providing practical estimates that take on no additional overhead.
- We provide a new bound on the score estimation error, extending the results of He et al. [2024], and, together with theoretical properties of diffusion-annealed Langevin dynamics [Cordero-Encinar et al., 2025a], establish convergence guarantees for our algorithm.
- We demonstrate the effectiveness of our sampler across different synthetic and real-world benchmarks.

Notation. We denote by $\|\cdot\|$ the Euclidean norm for vectors. We write by $\mathcal{N}(x; m, \mathbf{C})$ the density of a Gaussian random variable with mean m and covariance matrix \mathbf{C} evaluated at x . We let W_2 denote the Wasserstein-2 distance between probability measures [Villani, 2008]: $W_2^2(\mu, \nu) = \inf_{\gamma \in \Gamma(\mu, \nu)} \int \|x - y\|^2 d\gamma(x, y)$, where $\Gamma(\mu, \nu)$ is the set of couplings between μ and ν . We denote by $\text{KL}(\mu \parallel \nu)$ the Kullback-Leibler (KL) divergence between probability measures μ and ν .

2 Background

2.1 Diffusion Paths

Recent advances in diffusion models [Sohl-Dickstein et al., 2015, Ho et al., 2020, Song et al., 2021] have demonstrated that sampling paths based on carefully designed diffusion processes that bridge simple distributions to complex target distributions can effectively sample from very high-dimensional and multimodal targets. These paths, which we refer to as *diffusion paths*, are defined as a continuous-time family of distributions $(\mu_t)_{t \in [0, 1]}$ interpolating between a simple base distribution ν at time $t = 0$ and the target distribution π at time $t = 1$ [Chehab and Korba, 2024, Chehab et al., 2025, Cordero-Encinar et al., 2025a]. Specifically,

$$\mu_t(x) = \frac{1}{\sqrt{1 - \lambda_t^d}} \nu \left(\frac{x}{\sqrt{1 - \lambda_t}} \right) * \frac{1}{\sqrt{\lambda_t^d}} \pi \left(\frac{x}{\sqrt{\lambda_t}} \right), \quad (1)$$

for $t \in [0, 1]$ and a monotonically increasing schedule $\lambda_t \in [0, 1]$ with $\lambda_1 = 1$. Here, the random variables $X_t \sim \mu_t$ can be seen as the linear interpolation

$$X_t = \sqrt{1 - \lambda_t} Z + \sqrt{\lambda_t} X, \quad (2)$$

where $X \sim \pi$ and $Z \sim \nu$. The path in (1) is commonly instantiated with $\nu(x) = \mathcal{N}(x; 0, \sigma^2 \mathbf{I})$ for $\sigma > 0$ and $\lambda_t = \min\{1, \exp(-2T(1 - t))\}$, where T is a hyperparameter, as this results in μ_t coinciding with the time-reversed path marginals of an OU process [Chehab and Korba, 2024]. Samples can hence be propagated along the path by simulating the reverse process

$$dX_t = X_t dt + 2\nabla \log \mu_t(X_t) dt + \sqrt{2} dW_t, \quad (3)$$

for $t \in [0, 1]$ and $X_0 \sim \mu_0$. While convenient, the forward OU process requires an infinite time horizon to reach a Gaussian. A practical consequence is that T has to be chosen large enough so $\mu_0 \approx \nu$ but small enough to incur minimal discretisation errors for a fixed number of integration steps. We can alternatively consider schedules that reach both endpoints in finite time, i.e. with $\lambda_0 = 0$, in exchange for losing a closed-form analytical SDE description [Albergo et al., 2025]. The base density need not be Gaussian either, but we consider $\nu(x) = \mathcal{N}(x; 0, \sigma^2 \mathbf{I})$ for the remainder of the paper. To simulate this path, we turn to diffusion-annealed Langevin dynamics (DALD) [Guo et al., 2024, Cordero-Encinar et al., 2025a], which runs the SDE

$$dX_t = \nabla \log \hat{\mu}_t(X_t) dt + \sqrt{2} dW_t, \quad (4)$$

where $\hat{\mu}_t = \mu_{t/T}$, $t \in [0, T]$, and $X_0 \sim \nu$. Here, T controls how closely the SDE's true marginals track the reference path $(\mu_t)_{t \in [0,1]}$, i.e. a larger T results in slower dynamics that remain closer to the instantaneous target distributions.

Central to these dynamics is access to the score functions of path marginals. In fact, the path's convolutional structure admits two expressions for the score, known as the denoising score identity (DSI) [Vincent, 2011] and target score identity (TSI) [De Bortoli et al., 2024], respectively

$$\nabla \log \mu_t(x) = \mathbb{E}_{\varrho_{t,x}} \left[\frac{\sqrt{\lambda_t} Y - x}{\sigma^2(1 - \lambda_t)} \right] = \mathbb{E}_{\varrho_{t,x}} \left[\frac{-\nabla V_\pi(Y)}{\sqrt{\lambda_t}} \right] \quad (5)$$

where $V_\pi = -\log \pi$ is the target potential and $\varrho_{t,x}$ is the so-called posterior (conditional) distribution of the auxiliary variable Y given x in (2):

$$\varrho_{t,x}(y) \propto \nu \left(\frac{x - \sqrt{\lambda_t} y}{\sqrt{1 - \lambda_t}} \right) \pi(y). \quad (6)$$

While the score is generally intractable, it can be learned by a neural network [Vargas et al., 2024, Richter and Berner, 2024, Chen et al., 2025, Zhang and Chen, 2022, Noble et al., 2025] or approximated with a Monte Carlo estimate [Huang et al., 2024, Chen et al., 2024, Grenioux et al., 2024, Saremi et al., 2024, He et al., 2024, Cordero-Encinar et al., 2025b]. We follow the latter approach in this work.

2.2 Related Works

Diffusion-based samplers using Monte Carlo. Several works have utilised the SDE in (3) for sampling from unnormalised densities. Huang et al. [2024] use a combination of importance sampling and Langevin MCMC to estimate the score. They initialise their samples using a *Langevin-within-Langevin* procedure, where they undergo several steps of the unadjusted Langevin algorithm (ULA) to target μ_0 using Monte Carlo score estimates derived from approximate posterior samples propagated through ULA at the same time. Grenioux et al. [2024] builds upon this work by introducing a stochastic localisation framework with flexible denoising schedules and a discretisation scheme based on the signal-to-noise ratio (SNR) of the observation process (as in (2)). They start sampling at a later time, chosen as a hyperparameter, when both the path marginal and posterior are approximately log-concave. The reliance of these methods on MCMC, however, necessitates equilibration at every time step, creating a sequential bottleneck that cannot be overcome by simply increasing sample size. In an alternative line of work, He et al. [2024] propose rejection sampling for estimating the score, only making zero-order queries to the target density. While effective in low dimensions, the complexity of rejection sampling grows exponentially with the dimension, even for log-concave targets. Notably, the methods discussed all incur errors coming from their score estimation or SDE discretisation. Introducing a wrapper around reverse-diffusion based samplers, Wu et al. [2025] use the auxiliary variables from the posterior to estimate the path marginal density. From which, they propose a nested SMC sampler, RDSMC, where samples can be resampled to better adhere to the diffusion path marginals. In contrast, we employ an SMC sampler *only* for the auxiliary samples. While fundamentally different, our scheme provides unbiased estimates for the path marginal density, unlike the diffusion-based samplers discussed above, allowing it to be nested inside RDSMC.

Score identities. Some works have found convex combinations of the score identities to be beneficial towards the variance of loss objectives [De Bortoli et al., 2024, He et al., 2025]. The mixed score identity (MSI) is one example, assigning weights $1 - \lambda_t$ and λ_t to DSI and TSI, respectively. This choice is intuitive as the identities become unstable at opposite ends. A piecewise schedule is similarly justified [Cordero-Encinar et al., 2025b]. This leads us to examine more general schedules for weighting the identities and thereby minimising the variance of score estimates. Concurrent to our work, Kahouli et al. [2025] and Ko and Geffner [2025] propose a similar control variate score identity in the reverse diffusion context. However, their analyses do not provide practical estimates for arbitrary sampling targets, opting to work with Gaussian mixtures [Kahouli et al., 2025] or learning the schedule itself [Ko and Geffner, 2025]. Moreover, we choose to minimise the variance in expectation and additionally consider control-variates matrices.

3 Diffusion Path Sequential Monte Carlo

To numerically simulate the diffusion dynamics in (4), we discretise the time interval uniformly as $0 = t_0 < \dots < t_K = T$, where $t_k = \frac{kT}{K}$, leading to a sequence of distributions $(\hat{\mu}_{t_k})_{k=0}^K$. To sample from this path, we consider the Euler-Maruyama discretisation

$$X_{k+1} = X_k + h \nabla \log \hat{\mu}_{t_k}(X_k) + \sqrt{2h} \xi_k, \quad (7)$$

where $\xi_k \sim \mathcal{N}(0, I)$ and $h > 0$ is the step-size. This yields the annealed Langevin dynamics (ALD) sampler [Song and Ermon, 2019, Chehab and Korba, 2024, Cordero-Encinar et al., 2025a], which requires estimates of the time-varying score function. Estimating the score is an extremely challenging task when the target distribution is only known up to a normalising constant. We can, however, express the score in the following general form:

$$\nabla \log \hat{\mu}_{t_k}(x) = \mathbb{E}_{\varrho_{t_k/T,x}}[\varphi_{k,x}(Y)], \quad (8)$$

where $\varphi_{k,x} : \mathbb{R}^d \rightarrow \mathbb{R}^d$ is a vector-valued test function (choices of which can be judiciously made as we will discuss in Section 3.3) and $\varrho_{t_k/T,x}$ is the posterior distribution defined in (6). The time-varying expression in (8) naturally suggests an SMC scheme that evolves samples according to $(\varrho_{t_k/T,x})_{k=0}^K$, allowing Monte Carlo estimates for the score. To this end, we introduce a general SMC framework.

3.1 SMC Samplers for Score Estimation

We define a sequence of target distributions $(\rho_k)_{k=0}^K$, given by $\rho_k(\cdot) := \varrho_{t_k/T,x_k}(\cdot)$, where x_k is our sample at time t_k following ALD. To define the SMC sampler, we first define extended unnormalised distributions on the path space $\mathbb{R}^{d(k+1)}$

$$\tilde{\rho}_{0:k}(y_{0:k}) := \tilde{\rho}_k(y_k) \prod_{p=1}^k \mathsf{L}_{p-1}(y_p, y_{p-1}),$$

where $(\mathsf{L}_p)_{p=0}^{k-1}$ are a sequence of backward Markov kernels. It can be readily checked that the y_k -marginal of (normalised) $\rho_{0:k}$ is indeed ρ_k , justifying the choice of the extended target. Next, we define our proposal distribution on $\mathbb{R}^{d(k+1)}$ as

$$q_{0:k}(y_{0:k}) := q_0(y_0) \prod_{p=1}^k \mathsf{K}_p(y_{p-1}, y_p),$$

where q_0 is some initial auxiliary distribution and $(\mathsf{K}_p)_{p=1}^k$ are a sequence of forward Markov kernels. The resulting importance weights are given by

$$W_k(y_{0:k}) = \frac{\tilde{\rho}_{0:k}(y_{0:k})}{q_{0:k}(y_{0:k})} = W_{k-1}(y_{0:k-1}) G_k(y_{k-1}, y_k),$$

where we have the potential $G_k : \mathbb{R}^d \times \mathbb{R}^d \rightarrow \mathbb{R}_+$:

$$G_k(y_{k-1}, y_k) = \frac{\tilde{\rho}_k(y_k) \mathsf{L}_{k-1}(y_k, y_{k-1})}{\tilde{\rho}_{k-1}(y_{k-1}) \mathsf{K}_k(y_{k-1}, y_k)}. \quad (9)$$

Now, consider functions $\varphi_{k,x} : \mathbb{R}^d \rightarrow \mathbb{R}^d$ that form a score identity, i.e. $\nabla \log \hat{\mu}_{t_k}(x) = \mathbb{E}_{\rho_k}[\varphi_{k,x}(Y)]$, termed *score test functions*. Then, we have the following result through the Feynman-Kac identity [Del Moral, 2004, 2013]:

Proposition 1. *For any $k \geq 1$, let $Y_{0:k} \sim q_{0:k}$. If $\varphi_{k,x}$ forms a score identity as in (8), then we have*

$$\nabla \log \hat{\mu}_{t_k}(x_k) = \frac{\mathbb{E}[\varphi_{k,x_k}(Y_k) \prod_{p=0}^k G_p(Y_{p-1}, Y_p)]}{\mathbb{E}[\prod_{p=0}^k G_p(Y_{p-1}, Y_p)]},$$

where $G_0(y_{-1}, y_0) := \tilde{\rho}_0(y_0)/q_0(y_0)$ and the expectations are taken with respect to the path measure induced by the forward kernels $(\mathsf{K}_p)_{p=1}^k$ and initial distribution q_0 .

See Appendix A.1 for the proof. Proposition 1 therefore expresses the score as a ratio of expectations under the forward path measure, which can be estimated directly with an SMC sampler. Next, we outline our sampling method based on this construction.

3.2 The DPSMC Sampler

The previous framework leads us to introduce our diffusion path sequential Monte Carlo (DPSMC) sampler. We walkthrough a single iteration of our algorithm to demonstrate. At time t_{k-1} , we have: our sample X_{k-1} , propagated through ALD for $k-1$ steps using estimated scores; the weighted auxiliary variables $\{(W_{k-1}^i, Y_{k-1}^i)\}_{i=1}^N$, an output of our SMC sampler targeting ρ_{k-1} ; and a score estimate S_{k-1}^N , formed by a Monte Carlo approximation of (8) using the weighted auxiliary variables and the score test function $\varphi_{k-1, X_{k-1}}$. At time t_k , we first propagate our sample to X_k with an ALD step using the aforementioned score estimate. Then, we run one iteration of the SMC sampler to target ρ_k . This involves propagating each Y_{k-1}^i according to a forward kernel $K_k(\cdot | Y_{k-1}^i, X_k)$ and updating the weights with the potential in (9). We resample auxiliary variables if necessary to then obtain the new set of weighted samples $\{(W_k^i, Y_k^i)\}_{i=1}^N$ targeting ρ_k . A new score estimate S_k^N is produced using these new weighted samples and the score test function φ_{k, X_k} . The procedure is repeated until time t_{K-1} , after which we perform one final ALD step to obtain X_K . The overall procedure is summarised in Algorithm 1.

Algorithm 1 DPSMC (basic)

```

input  $\sigma, q_0, h = T/K, \phi_{k,x}$ 
1:  $X_0 \sim \mathcal{N}(0, \sigma^2 \mathbf{I})$ 
2:  $Y_0^i \sim q_0(\cdot)$  for all  $i \in [N]$ 
3:  $W_0^i = \exp(-V_\pi(Y_0^i))/q_0(Y_0^i)$  for all  $i \in [N]$ 
4:  $S_0^N = -X_0/\sigma^2$ 
5: for  $k = 1, \dots, K-1$  do
6:    $X_k \sim \mathcal{N}(\cdot; X_{k-1} + hS_{k-1}^N, 2h\mathbf{I})$  {ALD step}
7:   for  $i = 1, \dots, N$  do
8:      $\bar{Y}_k^i \sim K_k(\cdot | Y_{k-1}^i, X_k)$ 
9:      $W_k^i = W_{k-1}^i \frac{\bar{\rho}_k(\bar{Y}_k^i) \mathcal{L}_{k-1}(\bar{Y}_k^i, Y_{k-1}^i)}{\bar{\rho}_{k-1}(Y_{k-1}^i) K_k(Y_{k-1}^i, \bar{Y}_k^i)}$ 
10:    end for
11:    $w_k^i = \frac{W_k^i}{\sum_{j=1}^N W_k^j}$  for all  $i \in [N]$ 
12:    $S_k^N = \sum_{i=1}^N w_k^i \varphi_{k, X_k}(\bar{Y}_k^i)$  {Score estimation}
13:   if  $\widehat{\text{ESS}}(\{w_k^i\}_{i=1}^N) < N/2$  then
14:      $\{Y_k^i\}_{i=1}^N \sim \sum_{j=1}^N w_k^j \delta_{\bar{Y}_k^j}(\cdot)$  {Resampling}
15:      $W_k^i = 1$  for all  $i \in [N]$ 
16:   else
17:      $Y_k^i = \bar{Y}_k^i$  for all  $i \in [N]$ 
18:   end if
19: end for
20:  $X_K \sim \mathcal{N}(\cdot; X_{K-1} + hS_{K-1}^N, 2h\mathbf{I})$  {Final ALD step}
output  $X_K$ 

```

3.3 Score Test Functions

Now, we look at stable choices for test functions $\varphi_{k,x}$ that satisfy the score identity in (8). Building upon DSI and TSI, as in (5), we introduce a class of test functions

$$\phi_{t,x}^{\mathbf{A}}(y) := \frac{1}{\sqrt{1-\lambda_t}} \mathbf{A} \nabla \log \nu \left(\frac{x - \sqrt{\lambda_t} y}{\sqrt{1-\lambda_t}} \right) + \frac{1}{\sqrt{\lambda_t}} (\mathbf{I} - \mathbf{A}) \nabla \log \pi(y), \quad (10)$$

for $t \in [0, 1]$ and $\mathbf{A} \in \mathbb{R}^{d \times d}$. Such test functions can be used to build an estimator for the score, as they satisfy $\nabla \log \mu_t(x) = \mathbb{E}_{\varphi_{t,x}}[\phi_{t,x}^{\mathbf{A}}(Y)]$ (see Proposition A.1 for a proof). For the discrete-time scheme, at time step k , we accordingly have $\varphi_{k,x}(\cdot) = \phi_{t_k/T,x}^{\mathbf{A}}(\cdot)$.

We are interested in the variance behaviour of these test functions under the true marginals, parameterised by matrix schedules $\mathbf{A}_t \in \mathbb{R}^{d \times d}$. We refer to these as *control variate* (CV) schedules, since we can arrive at the same test function in (10) by introducing a control variate matrix (see Remark A.1). We first consider the case when $\mathbf{A}_t = \alpha_t \mathbf{I}$, i.e. a scalar weighting of DSI and TSI. The following result characterises the optimal choice of α_t for minimising the expected variance of the corresponding score estimator.

Proposition 2. *The scalar CV schedule $\alpha_t^* \in \mathbb{R}$ minimising the expected variance is given by*

$$\alpha_t^* = \underset{\alpha \in \mathbb{R}}{\operatorname{argmin}} \mathbb{E}_{X \sim \mu_t} [\operatorname{Var}_{Y \sim \varphi_{t,x}} [\phi_{t,x}^{\alpha \mathbf{I}}(Y)]] = \frac{\frac{1}{\lambda_t} \operatorname{Var}_\pi [\nabla \log \pi(X)]}{\frac{1}{1-\lambda_t} \operatorname{Var}_\nu [\nabla \log \nu(X)] + \frac{1}{\lambda_t} \operatorname{Var}_\pi [\nabla \log \pi(X)]},$$

where we write $\operatorname{Var}_p[f(X)] = \operatorname{Tr}(\operatorname{Cov}_p[f(X)])$.

See Appendix B.2.1 for the proof. This expression clearly decouples the dependence of time from the definition of the endpoint distributions. It aligns with our intuition of avoiding instabilities caused by the individual score identities, having α_t^* be non-increasing and going from one to zero. Unlike heuristic choices that start with DSI and end with TSI, this result shows explicitly when one is favoured over another, e.g. it is possible that $\alpha_t^* \approx 1$ for a majority of the time when the target has much larger score variance than the base. When they coincide in score variance, this reduces to $\alpha_t^* = 1 - \lambda_t$, i.e. MSI.

For arbitrary matrices, we have the following result.

Proposition 3. *The matrix CV schedule $\mathbf{A}_t^* \in \mathbb{R}^{d \times d}$ minimising the expected variance is given by*

$$\mathbf{A}_t^* = \underset{\mathbf{A} \in \mathbb{R}^{d \times d}}{\operatorname{argmin}} \mathbb{E}_{X \sim \mu_t} [\operatorname{Var}_{Y \sim \varrho_{t,X}} [\phi_{t,X}^{\mathbf{A}}(Y)]] = \frac{1}{\lambda_t} \mathcal{I}_{\pi} \left(\frac{1}{1 - \lambda_t} \mathcal{I}_{\nu} + \frac{1}{\lambda_t} \mathcal{I}_{\pi} \right)^{-1},$$

where \mathcal{I}_p denotes the covariance of the score of p , i.e.

$$\mathcal{I}_p := \operatorname{Cov}_p [\nabla \log p(X)] = \mathbb{E}_p [\nabla \log p(X) \nabla \log p(X)^T].$$

See Appendix B.2.3 for the proof. This optimal weighting accounts for the variance of individual score components and their pairwise covariances. Note the scalar schedule averages them out. We therefore expect a discrepancy between the scalar and matrix schedules when the base and target have a covariance mismatch, e.g. for extremely anisotropic targets. An example of this scenario is given in Figure 1, documenting the MSE evolution of different score identities. Ideally, one would choose base densities with a similar covariance structure as the target to maximise the effectiveness of scalar schedules.

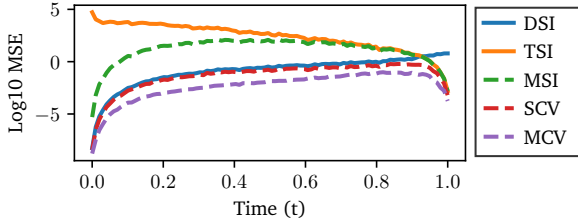


Figure 1: MSE of different score identities averaged across samples taken exactly from the diffusion path marginals and auxiliary variables from the corresponding conditional distribution. The target is chosen to be a bimodal mixture of anisotropic Gaussians. While MSI generally stays below the DSI/TSI upper envelope, the identities based on the scalar and matrix schedules, SCV and MCV, consistently remain under the lower envelope.

while practically being more stable, as all the auxiliary variables can be used for estimation. Besides, while our score estimates through SMC are biased due to self-normalisation, we empirically find that our schedules consistently improve the score estimates. This can be justified, since the variance of the unbiased estimator coincides with the asymptotic variance of the self-normalised estimator when the proposal matches the target.

3.4 Diffusion Path Design

Our diffusion path is parameterised by the schedule λ_t and the base Gaussian variance σ^2 . It is not surprising that poor choices for these parameters can render the sampler inefficient. For example, the schedule should spend more time where the path is rapidly changing and less where it does not. Intuition also suggests that σ^2 should not be too small else $\mu_t(x) \approx \pi(x/\sqrt{\lambda_t})/\sqrt{\lambda_t^d}$, causing the mode structure to be determined within a few time steps and the remainder of the path to be spent dilating the modes. It should not be too large either, or the marginals are indistinguishable from a Gaussian for most of the path.

To select a value for σ^2 , we consult the SNR of our intermediate random variables in (2). We define the SNR as

$$\text{SNR}(t) := \frac{\mathbb{E} [\|\sqrt{\lambda_t} X\|^2]}{\mathbb{E} [\|\sqrt{1 - \lambda_t} Z\|^2]} = \frac{\mathbb{E}_\pi [\|X\|^2] \lambda_t}{\sigma^2 d (1 - \lambda_t)},$$

using the power or second moment of the target $\mathbb{E}_\pi [\|X\|^2]$ as opposed to its scalar variance [Grenioux et al., 2024]. Here, choosing $\sigma^2 \propto \mathbb{E}_\pi [\|X\|^2]/d$ yields an SNR independent of the target. We set $\sigma^2 = \mathbb{E}_\pi [\|X\|^2]/d$, as it is the most natural choice, keeping the second moment fixed across the path marginals.

Now, we seek a λ_t schedule. A natural choice would be the linear schedule $\lambda_t = t$. One can justify this as linearly interpolating the ratio between the signal power and the total power under our variance choice. Although, this construction does not explicitly capture our intuition of spending more time where the path evolves quickly. Let $\mu = (\mu_t)_{t \in [0,1]}$ denote the curve of probability measures corresponding to the diffusion path. We can consider the action functional \mathcal{A} as a measure of how rapidly the path marginals evolve throughout the curve. It is defined as

$$\mathcal{A}(\mu) = \int_0^T |\dot{\mu}|_t^2 dt, \quad (11)$$

where $|\dot{\mu}|_t = \lim_{\delta \rightarrow 0} W_2(\mu_{t+\delta}, \mu_t)/|\delta|$ is the metric derivative of μ at time t . This quantity upper bounds the KL divergence between the target and the final marginal distribution of ALD [Guo et al., 2024, Cordero-Encinar et al., 2025a] (see Appendix C.1 for details). Choosing λ_t that minimises (11) is therefore a natural choice. Since a closed-form solution for the action is generally unavailable, we select λ_t that minimises the following upper bound functional

$$\mathcal{A}(\mu) \leq \int_0^T \left(\frac{\sigma^2 d}{4(1 - \lambda_t)} + \frac{\mathbb{E}_\pi [\|X\|^2]}{4\lambda_t} \right) (\partial_t \lambda_t)^2 dt.$$

When $\sigma^2 d = \mathbb{E}_\pi [\|X\|^2]$, the minimiser is available analytically and is given by

$$\lambda_t^* = \sin^2 \left(\frac{\pi t}{2} \right) = 1 - \cos^2 \left(\frac{\pi t}{2} \right),$$

which is the well-known cosine schedule (see Appendix C.2 for the proof). This schedule eases in and out, allowing more time at the start for samples to localise in modes at the right proportion and at the end for details to be gradually refined. Unlike the linear schedule, this also provides a handy finite upper bound on the action.

As a remark, our choices have been made with respect to the diffusion path alone, which is but one aspect of the sampler's construction. These choices also influence the path of posteriors $\varrho_{t,x}$, whose smooth evolution is vital for getting high-quality auxiliary variables and therefore accurate score estimates. We reserve this analysis for future work and instead adopt an orthogonal approach to improving score estimates, as discussed in the previous section.

3.5 Algorithmic Choices and Modifications

Using the results we presented, we briefly detail our implementation of the DPSMC algorithm in practice.

Initialisation. We choose to initialise the auxiliary variables according to $q_0(x) = \mathcal{N}(x; 0, \tilde{\sigma}^2 \mathbf{I})$, where $\tilde{\sigma}^2$ incorporates some information about the target. We follow Grenioux et al. [2024] in setting $\tilde{\sigma}^2 = R^2 d + \tau^2$, where we assume the target can be decomposed as a convolution between $\mathcal{N}(0, \tau^2 \mathbf{I})$ and a distribution compactly supported on $B(\mathbb{E}_\pi [\|X\|^2], R^2 d)$. If these quantities are unavailable, we instead opt for $\tilde{\sigma}^2 = \mathbb{E}_\pi [\|X\|^2]/d$. These choices allow the auxiliary variables to generally coincide with regions of high density in the target. Of course, this has some limitations, and these are addressed in a later paragraph. Notably, we do not perform any Langevin-within-Langevin procedures, as our path marginals start from a Gaussian.

Propagation. We propagate auxiliary variables according to a Metropolis-adjusted Langevin algorithm (MALA) kernel K_k^{MALA} with an adaptive step size, geometrically adjusted to maintain a global acceptance

ratio, as in Grenioux et al. [2024]. We choose to do only one step of MALA per iteration. Using our full ensemble of samples and auxiliary variables, we estimate the target covariance and, hence, the optimal matrix CV schedule in Proposition 3. Together with the test function in (10), we estimate scores for our samples.

Our practical implementation of DPSMC is given in Algorithm 2 in Appendix. While our samples are interacting in step size adaptation and target score covariance estimation, one could first estimate these underlying quantities and consider the non-interacting version of our sampler using these settings. Overall, our scheme is relatively straightforward with T being our only critical hyperparameter.

Taming terminal instabilities. While our scheme allows for single MALA steps per iteration, this shortens the time for auxiliary variables to equilibrate themselves with respect to the next target. This can be detrimental when the samples evolving via ALD make large jumps, especially towards the end when the posterior contracts to a Dirac centred at these samples. In the absence of a finer discretisation, we turn to a simple heuristic that we find to work well empirically. It turns out that we consistently maintain our target acceptance ratio up to some tolerance, right until the posterior's Gaussian component dominates. When T is chosen to be too large, the acceptance ratio eventually goes to zero. We heuristically halt the SMC sampler when the acceptance ratio goes below a threshold and substitute the score estimates with the target score itself.

Tempering the posterior path. Our initialisation is no silver bullet as one might expect. If not chosen carefully, a single auxiliary variable can dominate the importance weights, or some target modes may be missed. To address this, we loosely exploit Proposition 4 in the next section, which informally says we can keep score errors within $\mathcal{O}(\varepsilon^2)$ if the law of our auxiliary variables are within $\mathcal{O}(\varepsilon/\sqrt{\lambda_{t_k}/T})$ in W_2 distance from the posterior at time k . This means, while $\varrho_{0,x}(y) = \pi(y)$, we are allowed to have a crude set of weighted samples that approximate it in expectation. This allowance allows us to trade some bias for ease in sampling. We consider an increasing inverse-temperature schedule $0 < \beta_0 < \dots < \beta_K = 1$ and construct an alternative path of intermediate targets $\tilde{\rho}_k^\beta(y) \propto \tilde{\rho}_k(y)^{\beta_k}$. Our premise for an increasing schedule is to encourage exploration at the start and gradually reduce the bias caused by targeting the tempered posterior, as depicted in Figure 2. Note that samples are reweighted when estimating the score. The updated algorithm is given in Algorithm 5 in Appendix. This scheme is explored in conjunction with the normal DPSMC algorithm.

4 Theoretical Analysis

In this section, we analyse the different sources of error in our algorithm, building on the theoretical analysis of diffusion-annealed Langevin Monte Carlo (DALMC) presented in Cordero-Encinar et al. [2025a]. We first introduce the required assumptions.

Assumption 1. *The target distribution has density with respect to Lebesgue, $\pi \propto e^{-V_\pi} \in \mathcal{P}(\mathbb{R}^d)$, and satisfies*

- (i) *Finite second-order moment, $M_2 := \mathbb{E}_\pi[\|X\|^2] < \infty$*
- (ii) *V_π has Lipschitz continuous gradients, with Lipschitz constant L_π .*
- (iii) *Strong convexity outside of a compact: $\exists R > 0$ such that $\inf_{\|x\| \geq R} \nabla^2 V_\pi \succ 0$.*

Note that this assumption extends the commonly used assumption Grenioux et al. [2024], Saremi et al. [2024] that π is given by the convolution of a compactly supported measure and a Gaussian distribution. Moreover, under Assumption 1, it follows from Cordero-Encinar et al. [2025a, Lemma 3.2] and Cattiaux et al. [2025, Lemma 3.8] that $\nabla \log \mu_t$ is Lipschitz continuous with finite constant L_t , satisfying $\sup_t L_t \leq L$.

To bound the KL divergence between the target π and the final distribution p_K obtained by the DPSMC algorithm, we need to control the score estimation error. Assume that we obtain $X_k \sim \hat{\mu}_t$ perfectly and

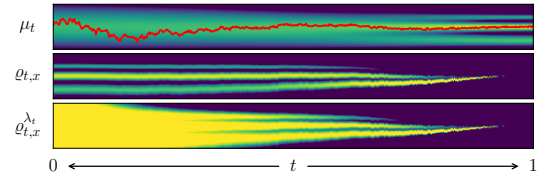


Figure 2: Tempering the posterior path allows better exploration at initial time steps, trading bias in score estimates (which we are allowed to have to some degree) for ease in sampling.

then generate the weighted particles $\{(w_k^i, \bar{Y}_k^i)\}_{i=1}^N$. For simplicity, we consider the scalar CV schedule and denote $\alpha_k^* := \alpha_{t_k/T}^*$ and $\lambda_k := \lambda_{t_k/T}$. We define the score estimator

$$S_k^N(X_k) := \sum_{i=1}^N w_k^i \phi_{t_k/T, X_k}^{\alpha_k^* \mathbf{I}}(\bar{Y}_k^i). \quad (12)$$

The following proposition provides a bound on this error.

Proposition 4 (Score estimation error). *Suppose Assumption 1 holds. Let $\{X_k\}_{k=1}^K$ such that $\hat{\mu}_{t_k} = \mathcal{L}(X_k)$ for all $k = 1, \dots, K$. Consider the score estimator $S_k^N(X_k)$ defined in (12) using a weighted particle system $\{(w_k^i, \bar{Y}_k^i)\}_{i=1}^N$ such that $\mathbb{E}[W_2^2(\sum w_k^i \delta_{\bar{Y}_k^i}, \varrho_{t_k/T, X_k})] \leq \delta(k, N)^2$ for all $k \geq 0$, then we have*

$$\mathbb{E} [\|\nabla \log \hat{\mu}_{t_k}(X_k) - S_k^N(X_k)\|^2] \leq 2\delta(k, N)^2 \left((\alpha_k^*)^2 \frac{\lambda_k}{(1 - \lambda_k)^2} + (1 - \alpha_k^*)^2 \frac{L_\pi^2}{\lambda_k} \right).$$

See Appendix D.1 for the proof. This result generalises Proposition 3.1 in He et al. [2024], which can be recovered by setting $\alpha_k^* = 1$ for all k and using a system of equally weighted i.i.d particles. For small values of k , λ_k is small and α_k^* is close to 1. In particular, $\alpha_k^* = 1 - \lambda_k$ when the score variances of ν and π coincide. The terms inside the parentheses are of order $\mathcal{O}(\lambda_k)$, which implies that choosing $\delta(k, N) = \mathcal{O}(\varepsilon/\sqrt{\lambda_k})$ provides a bound on the first term of order $\mathcal{O}(\varepsilon^2)$. This suggests that while $\varrho_{t_k/T, x}$ is difficult to sample from for small k (since $\varrho_{0,x}(y) = \pi(y)$), relatively large approximation errors (of order $\mathcal{O}(\varepsilon/\sqrt{\lambda_k})$) between the distribution of our auxiliary variables and $\varrho_{t_k/T, x}$ can still result in a reliable score estimator when measured in the L^2 sense. In other words, poorly sampled SMC particles in the initial steps do not significantly degrade the score error.

We can apply Proposition 4 to obtain a bound on the score estimation error for our weighted estimator (12). In particular, if we require the score estimation error over time to be bounded by $\varepsilon_{\text{score}}^2$, then the bound in (13) guides the choice of $\delta(k, N)$ such that

$$\sum_{k=0}^{K-1} h \mathbb{E} [\|\nabla \log \hat{\mu}_{t_k}(X_k) - \hat{s}_k(X_k)\|^2] \leq \varepsilon_{\text{score}}^2.$$

This allows us to invoke Theorem 3.4 in Cordero-Encinar et al. [2025a] to bound the final error of the algorithm. In particular, we have the following result.

Theorem 1. *Under Assumption 1, the DPSMC algorithm initialised at $X_0 \sim \nu$ satisfies*

$$\text{KL}(\pi \parallel p_K) \lesssim \left(1 + \frac{L^2 T^4}{K^2}\right) \frac{M_2 + d}{T} + \frac{d L^2 T^2}{K} \left(1 + \frac{L T}{K}\right) + \varepsilon_{\text{score}}^2.$$

This bound implies that, for $\varepsilon = \mathcal{O}(\varepsilon_{\text{score}})$, and under the choices $K = \mathcal{O}\left(\frac{d(M_2 \vee d)^2 L^2}{\varepsilon_{\text{score}}^2}\right)$ and $T = \mathcal{O}\left(\frac{\varepsilon_{\text{score}}^2}{M_2 \vee d}\right)$, we can keep $\text{KL}(\pi \parallel p_K) \leq \varepsilon^2$.

5 Experiments

We now test DPSMC across several benchmark targets alongside other samplers. Table 1 summarises our findings.

Samplers. We compare our methods against several classical samplers: annealed importance sampling (AIS) [Neal, 2001] and SMC [Del Moral et al., 2006], as well as those based on reverse-diffusion, RDMC [Huang et al., 2024] and SLIPS [Grenioux et al., 2024]. Details on their hyperparameter selections and setup are in Appendix F.1. We fix the number of energy evaluations for all samplers, except RDMC, where it has twice as many, following its original implementation. We also globally fix the number of discretisation steps to $K = 1024$, unless otherwise stated. We test several instances of our method: the original algorithm (DPSMC), its version where auxiliary variables evolve according to a tempered

Algorithm	Batched Evals (↓)	GMM40 ($d = 2$) (↓)	GMM40 ($d = 50$) (↓)	Rings ($d = 2$) (↓)	Funnel ($d = 10$) (↓)	Ionosphere ($d = 35$) (↑)	Sonar ($d = 61$) (↑)
AIS	131K	2.35 ± 0.41	115.13 ± 2.98	0.19 ± 0.01	0.037 ± 0.003	-87.79 ± 0.10	-110.94 ± 0.10
SMC	131K	5.50 ± 0.22	111.81 ± 4.84	$\mathbf{0.18 \pm 0.01}$	0.035 ± 0.003	-87.79 ± 0.10	-110.94 ± 0.10
RDMC [Huang et al., 2024]	32K	12.35 ± 0.11	79.37 ± 0.10	0.29 ± 0.02	0.082 ± 0.003	-109.97 ± 0.23	-129.82 ± 0.18
SLIPS [Grenioux et al., 2024]	32K	4.10 ± 0.30	$\mathbf{27.01 \pm 1.32}$	$\mathbf{0.18 \pm 0.01}$	0.073 ± 0.003	-87.88 ± 0.10	-110.88 ± 0.06
DPSMC	1K	1.92 ± 0.12	28.80 ± 1.59	0.20 ± 0.02	0.062 ± 0.003	$\mathbf{-83.92 \pm 0.09}$	$\mathbf{-108.84 \pm 0.09}$
DPSMC w/ Tempering	1K	1.67 ± 0.26	29.45 ± 1.35	0.20 ± 0.01	0.121 ± 0.003	-83.97 ± 0.10	$\mathbf{-108.62 \pm 0.10}$
DPSMC w/ 8x Discretisation	8K	1.24 ± 0.13	28.44 ± 1.68	0.18 ± 0.01	0.031 ± 0.002	-86.48 ± 0.10	-110.09 ± 0.10

Table 1: Performance of algorithms on toy targets and Bayesian logistic regression datasets across 10 seeds. Results with the best performance are highlighted in **bold** and those in second-best are underlined. The second column indicates the number of batched energy evaluations made by each sampler—this is often a reliable metric for measuring runtimes in the regime where hardware capacity matches or exceeds the batch size requirements. Metrics for benchmarks: entropy-regularised W_2 ($\epsilon = 0.05$) for GMM40 and Rings, Kolmogorov-Smirnov (KS) distance for Funnel, and predictive likelihood for Ionosphere and Sonar.

posterior path with $\beta_k = \max\{\lambda_k, 10^{-2}\}$ (DPSMC w/ Tempering), and a version with a finer discretisation ($K \rightarrow 8K$) but fewer auxiliary variables ($N \rightarrow N/8$) (DPSMC w/ 8x Discretisation). Each sampler, where applicable, is informed of the target geometry per Grenioux et al. [2024] and assessed on the 4096 samples they produce across 10 seeds.

Toy target distributions. We consider several toy targets that test a sampler’s ability to tackle multimodality and complicated geometries. Our first example is GMM40, a uniform mixture of 40 Gaussians with identity covariance and means randomly sampled from a d -dimensional hypercube of length 40 under a fixed seed. We consider $d = 2$ and $d = 50$. We also test targets with challenging geometries such as Rings ($d = 2$) Grenioux et al. [2024], where regions of high density are localised along four concentric rings, and Funnel ($d = 10$) Neal [2001], which consists of an exponentially narrowing funnel. We evaluate the quality of samples relative to the target through their entropy-regularised W_2 distance ($\epsilon = 0.05$) for GMM40 and Rings and the sliced Kolmogorov-Smirnov (KS) distance for Funnel.

Bayesian logistic regression. Unlike some of our pathological targets aimed at stress-testing samplers, posterior sampling from a Bayesian logistic regression model showcases how samplers deal with high-dimensional real-world datasets. We consider this problem using the Ionosphere ($d = 35$) and Sonar ($d = 61$) datasets. Samples, i.e. weights of the model, are evaluated based on their predictive likelihood on a held out test dataset.

Our results suggest that DPSMC is competitive with existing samplers on the full range of benchmarks. It especially excels in Bayesian logistic regression problems, likely due to the Gaussian prior on the model weights coinciding with our initialisation. Our tempering scheme improved exploration of the posterior landscape at the cost of increased bias and variance in score estimates. This tradeoff was beneficial for benchmarks with poor initial coverage but unnecessary for those with already sufficient ones. In some problems, DPSMC was more effective with a finer discretisation, despite having fewer auxiliary variables. We believe these were settings where score estimation performance had saturated, and gains had to come from a finer ALD dynamics.

We find DPSMC has speed-ups of several orders of magnitude compared to other samplers while achieving better if not minimal deterioration in sample quality. In the modern age of GPUs and parallel computing, inference at scale is primarily achieved through distributing work horizontally, i.e. across a cluster of devices, and has significantly rewarded methods that can leverage this [Vaswani et al., 2017, Chen et al., 2023]. We argue that a sampler’s *ability to batch energy evaluations* is hence an increasingly important design axis. In essence, methods that can exploit this batching for estimating better transport paths can achieve better wall-clock times and sample quality, even if they use more energy evaluations. DPSMC achieves this by largely remaining non-equilibrium in all its components. Methods relying on MCMC, however, require sufficient equilibration, e.g. for intricate targets such as those in Figure 3.

6 Discussion

We have developed diffusion path sequential Monte Carlo (DPSMC), a sampler based on diffusion-annealed Langevin dynamics using SMC as a backbone for score estimation. To improve its efficacy, we introduced control-variate schedules and motivated a principled parameterisation of the diffusion path. We provided theoretical guarantees for DPSMC, accounting for score estimation and discretisation errors. We then demonstrated that it is competitive with other samplers across a range of benchmark targets while maintaining a high degree of batch parallelism. Throughout, we opted to keep our setup simple where possible. DPSMC is quite general, however, and can be extended along several promising fronts. Robust initialisation schemes for auxiliary variables, e.g. coarsely discretised AIS, can be explored to alleviate a limitation of our current scheme of using simple importance sampling. Sample dynamics can also be improved through better discretisation schemes, an SMC correction per RDSMC, or an under-damped version of ALD.

Acknowledgements

J.M.Y. is supported by the Roth Scholarship provided by the Department of Mathematics, Imperial College London. P.C.E. is funded by EPSRC through the Centre for Doctoral Training in Modern Statistics and Statistical Machine Learning (StatML), grant no. EP/S023151/1. S.R.’s work is partially funded by the Deutsche Forschungsgemeinschaft (DFG) under Project-ID 318763901 – SFB1294. Lastly, J.M.Y. would like to thank Tim Wang for helpful discussions.

References

Michael Albergo, Nicholas M. Boffi, and Eric Vanden-Eijnden. Stochastic interpolants: A unifying framework for flows and diffusions. *Journal of Machine Learning Research*, 26(209):1–80, 2025.

Christopher M Bishop and Nasser M Nasrabadi. *Pattern recognition and machine learning*, volume 4. Springer, 2006.

Patrick Cattiaux, Paula Cordero-Encinar, and Arnaud Guillin. Diffusion annealed langevin dynamics: a theoretical study. *arXiv preprint arXiv:2511.10406*, 2025.

Omar Chehab and Anna Korba. A practical diffusion path for sampling. In *ICML Workshop on Structured Probabilistic Inference & Generative Modeling*, 2024.

Omar Chehab, Anna Korba, Austin Stromme, and Adrien Vacher. Provable convergence and limitations of geometric tempering for langevin dynamics. In *International Conference on Learning Representations (ICLR)*. arXiv, 2025.

Charlie Chen, Sebastian Borgeaud, Geoffrey Irving, Jean-Baptiste Lespiau, Laurent Sifre, and John Jumper. Accelerating large language model decoding with speculative sampling, 2023. URL <https://arxiv.org/abs/2302.01318>.

Junhua Chen, Lorenz Richter, Julius Berner, Denis Blessing, Gerhard Neumann, and Anima Anandkumar. Sequential Controlled Langevin Diffusions. In *The Thirteenth International Conference on Learning Representations*, 2025.

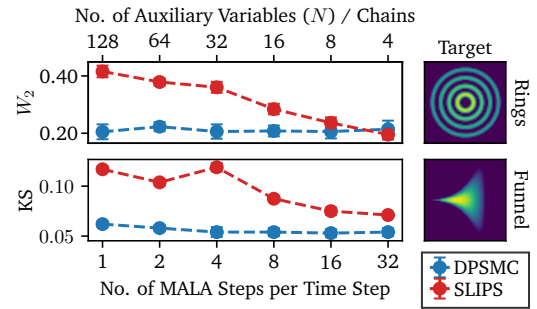


Figure 3: Densities with intricate geometries demand several MALA steps for MCMC-based methods like SLIPS. Here, the number of particles or chains is adjusted for each method so the total number of energy evaluations is fixed. The discretisation is also fixed.

Wenlin Chen, Mngtian Zhang, Brooks Paige, José Miguel Hernández-Lobato, and David Barber. Diffusive gibbs sampling. In *Forty-first International Conference on Machine Learning*, 2024.

Paula Cordero-Encinar, O Deniz Akyildiz, and Andrew B Duncan. Non-asymptotic analysis of diffusion annealed langevin monte carlo for generative modelling. *arXiv preprint arXiv:2502.09306*, 2025a.

Paula Cordero-Encinar, Andrew B Duncan, Sebastian Reich, and O Deniz Akyildiz. Sampling by averaging: A multiscale approach to score estimation. In *The Thirty-ninth Annual Conference on Neural Information Processing Systems*, 2025b.

Valentin De Bortoli, Michael Hutchinson, Peter Wirsberger, and Arnaud Doucet. Target score matching. *arXiv preprint arXiv:2402.08667*, 2024.

Pierre Del Moral. *Feynman-Kac formulae: genealogical and interacting particle systems with applications*. Springer, 2004.

Pierre Del Moral. Mean field simulation for monte carlo integration. *Monographs on Statistics and Applied Probability*, 126(26):6, 2013.

Pierre Del Moral, Arnaud Doucet, and Ajay Jasra. Sequential monte carlo samplers. *Journal of the Royal Statistical Society Series B: Statistical Methodology*, 68(3):411–436, 2006.

Andrew Gelman, John B Carlin, Hal S Stern, and Donald B Rubin. *Bayesian data analysis*. Chapman and Hall/CRC, 1995.

Charles J Geyer and Elizabeth A Thompson. Annealing markov chain monte carlo with applications to ancestral inference. *Journal of the American Statistical Association*, 90(431):909–920, 1995.

Paul Glasserman. *Monte Carlo methods in financial engineering*, volume 53. Springer, 2004.

Louis Grenioux, Maxence Noble, Marylou Gabré, and Alain Oliviero Durmus. Stochastic localization via iterative posterior sampling. In *International Conference on Machine Learning*, pages 16337–16376. PMLR, 2024.

Wei Guo, Molei Tao, and Yongxin Chen. Provable benefit of annealed langevin monte carlo for non-log-concave sampling. *arXiv preprint arXiv:2407.16936*, 2024.

Jiajun He, Wenlin Chen, Mngtian Zhang, David Barber, and José Miguel Hernández-Lobato. Training neural samplers with reverse diffusive kl divergence. In *International Conference on Artificial Intelligence and Statistics*, pages 5167–5175. PMLR, 2025.

Ye He, Kevin Rojas, and Molei Tao. Zeroth-order sampling methods for non-log-concave distributions: Alleviating metastability by denoising diffusion. *Advances in Neural Information Processing Systems*, 37: 71122–71161, 2024.

Jonathan Ho, Ajay Jain, and Pieter Abbeel. Denoising diffusion probabilistic models. *Advances in neural information processing systems*, 33:6840–6851, 2020.

Xunpeng Huang, Hanze Dong, Yifan Hao, Yian Ma, and Tong Zhang. Reverse Diffusion Monte Carlo. In *The Twelfth International Conference on Learning Representations*, 2024.

Khaled Kahouli, Romuald Elie, Klaus-Robert MÃžller, Quentin Berthet, Oliver T Unke, and Arnaud Doucet. Control variate score matching for diffusion models. *arXiv preprint arXiv:2512.20003*, 2025.

Ioannis Karatzas and Steven E. Shreve. *Brownian Motion and Stochastic Calculus*. Springer New York, NY, 1991.

Joohwan Ko and Tomas Geffner. Latent target score matching, with an application to simulation-based inference. In *Machine Learning and the Physical Sciences Workshop, NeurIPS*, 2025.

Radford M Neal. Annealed importance sampling. *Statistics and computing*, 11(2):125–139, 2001.

Radford M Neal. Slice sampling. *The annals of statistics*, 31(3):705–767, 2003.

Radford M Neal et al. MCMC using Hamiltonian dynamics. *Handbook of markov chain monte carlo*, 2(11): 2, 2011.

Mark EJ Newman and Gerard T Barkema. *Monte Carlo methods in statistical physics*. Clarendon Press, 1999.

Maxence Noble, Louis Grenioux, Marylou Gabré, and Alain Oliviero Durmus. Learned reference-based diffusion sampler for multi-modal distributions. In *The Thirteenth International Conference on Learning Representations*, 2025.

Lorenz Richter and Julius Berner. Improved sampling via learned diffusions. In *The Twelfth International Conference on Learning Representations*, 2024.

Saeed Saremi, Ji Won Park, and Francis Bach. Chain of log-concave markov chains. In *The Twelfth International Conference on Learning Representations*, 2024.

Jascha Sohl-Dickstein, Eric Weiss, Niru Maheswaranathan, and Surya Ganguli. Deep unsupervised learning using nonequilibrium thermodynamics. In *International conference on machine learning*, pages 2256–2265. pmlr, 2015.

Yang Song and Stefano Ermon. Generative modeling by estimating gradients of the data distribution. *Advances in neural information processing systems*, 32, 2019.

Yang Song, Jascha Sohl-Dickstein, Diederik P. Kingma, Abhishek Kumar, Stefano Ermon, and Ben Poole. Score-Based Generative Modeling through Stochastic Differential Equations. In *International Conference on Learning Representations*, 2021.

Robert H Swendsen and Jian-Sheng Wang. Replica monte carlo simulation of spin glasses. *Physical review letters*, 57(21):2607–2609, 1986.

B (Bruce) Van Brunt. *The calculus of variations / Bruce van Brunt*. Universitext. Springer, New York, 2003.

Francisco Vargas, Shreyas Padhy, Denis Blessing, and Nikolas Nüsken. Transport meets Variational Inference: Controlled Monte Carlo Diffusions. In *The Twelfth International Conference on Learning Representations*, 2024.

Ashish Vaswani, Noam Shazeer, Niki Parmar, Jakob Uszkoreit, Llion Jones, Aidan N Gomez, Łukasz Kaiser, and Illia Polosukhin. Attention is all you need. *Advances in neural information processing systems*, 30, 2017.

Cédric Villani. *Optimal transport: old and new*, volume 338. Springer, 2008.

Pascal Vincent. A connection between score matching and denoising autoencoders. *Neural computation*, 23(7):1661–1674, 2011.

Darren J Wilkinson. *Stochastic modelling for systems biology*. Chapman and Hall/CRC, 2018.

Luhuan Wu, Han Yi, Christian Naesseth, and John Cunningham. Reverse Diffusion Sequential Monte Carlo Samplers. In *Conference on Neural Information Processing Systems*, 2025.

Qinsheng Zhang and Yongxin Chen. Path integral sampler: A stochastic control approach for sampling. In *International Conference on Learning Representations*, 2022.

Organisation of the appendix

We present proofs for propositions stated in the main text as well as supplementary information, such as implementation details and additional experiments. The appendix is organised as follows:

- A. Sequential Monte Carlo samplers
- B. Score Test Functions
- C. Diffusion Path Design
- D. Theoretical Analysis
- E. DPSMC Implementation
- F. Numerical Experiments
- G. Additional Experiments

A Sequential Monte Carlo samplers

In this section, we show certain SMC results which we have used in the paper.

A.1 Proof of Proposition 1

Proposition 1. *For any $k \geq 1$, let $Y_{0:k} \sim q_{0:k}$. If $\varphi_{k,x}$ forms a score identity as in (8), then we have*

$$\nabla \log \hat{\mu}_{t_k}(x_k) = \frac{\mathbb{E}[\varphi_{k,x_k}(Y_k) \prod_{p=0}^k G_p(Y_{p-1}, Y_p)]}{\mathbb{E}[\prod_{p=0}^k G_p(Y_{p-1}, Y_p)]},$$

where $G_0(y_{-1}, y_0) := \tilde{\rho}_0(y_0)/q_0(y_0)$ and the expectations are taken with respect to the path measure induced by the forward kernels $(K_p)_{p=1}^k$ and initial distribution q_0 .

Proof. Expanding the product we have that

$$\prod_{p=0}^k G_p(y_{p-1}, y_p) = \frac{\tilde{\rho}_0(y_0)}{q_0(y_0)} \prod_{p=1}^k \frac{\tilde{\rho}_p(y_p) L_{p-1}(y_p, y_{p-1})}{\tilde{\rho}_{p-1}(y_{p-1}) K_p(y_{p-1}, y_p)} = \frac{\tilde{\rho}_k(y_k) \prod_{p=1}^k L_{p-1}(y_p, y_{p-1})}{q_0(y_0) \prod_{p=1}^k K_p(y_{p-1}, y_p)} = \frac{\tilde{\rho}_{0:k}(y_{0:k})}{q_{0:k}(y_{0:k})}.$$

The ratio in the proposition is therefore given by

$$\begin{aligned} \frac{\mathbb{E}[\varphi_{k,x_k}(Y_k) \prod_{p=1}^k G_p(Y_{p-1}, Y_p)]}{\mathbb{E}[\prod_{p=1}^k G_p(Y_{p-1}, Y_p)]} &= \frac{\int q_{0:k}(y_{0:k}) \varphi_{k,x_k}(y_k) \frac{\tilde{\rho}_{0:k}(y_{0:k})}{q_{0:k}(y_{0:k})} dy_{0:k}}{\int q_{0:k}(y_{0:k}) \frac{\tilde{\rho}_{0:k}(y_{0:k})}{q_{0:k}(y_{0:k})} dy_{0:k}} = \frac{\int \tilde{\rho}_{0:k}(y_{0:k}) \varphi_{k,x_k}(y_k) dy_{0:k}}{\int \tilde{\rho}_{0:k}(y_{0:k}) dy_{0:k}} \\ &= \int \rho_{0:k}(y_{0:k}) \varphi_{k,x_k}(y_k) dy_{0:k} = \int \rho_k(y_k) \varphi_{k,x_k}(y_k) dy_k, \end{aligned}$$

where we have used the fact that $\rho_{0:k}(y_{0:k})$ admits $\rho_k(y_k)$ as a marginal. Since $\rho_k(\cdot) = \varrho_{t_k/T,x_k}(\cdot)$ and our test function $\varphi_{k,x}$ satisfies (8) for any $x \in \mathbb{R}^d$, then we can conclude that

$$\frac{\mathbb{E}[\varphi_{k,x}(Y_k) \prod_{p=1}^k G_p(Y_{p-1}, Y_p)]}{\mathbb{E}[\prod_{p=1}^k G_p(Y_{p-1}, Y_p)]} = \mathbb{E}_{\varrho_{t_k/T,x_k}}[\varphi_{k,x_k}(Y_k)] = \nabla \log \hat{\mu}_{t_k}(x_k).$$

□

A.2 Weight update for $\mathsf{K}_k^{\text{MALA}}$ choice

In Section 3.1, we derived our incremental weight function for general kernels $(\mathsf{K}_p)_{p=1}^k$ and $(\mathsf{L}_{p-1})_{p=1}^k$ as

$$G_k(y_{k-1}, y_k) = \frac{\tilde{\rho}_k(y_k) \mathsf{L}_{k-1}(y_k, y_{k-1})}{\tilde{\rho}_{k-1}(y_{k-1}) \mathsf{K}_k(y_{k-1}, y_k)}. \quad (13)$$

As we mentioned in Section 3.5, we choose the forward kernel to be the MALA kernel which simplifies the weights. In order to see this, if K_k leaves ρ_k invariant and we can choose the backward kernel as its time-reversal,

$$\mathsf{L}_{k-1}(y_k, y_{k-1}) = \frac{\rho_k(y_{k-1}) \mathsf{K}_k(y_{k-1}, y_k)}{\rho_k(y_k)}, \quad (14)$$

then the incremental weight simplifies, which yields the familiar annealed importance sampling weights. In particular, we can write

$$\begin{aligned} G_k(y_{k-1}, y_k) &= \frac{\tilde{\rho}_k(y_k) \mathsf{L}_{k-1}(y_k, y_{k-1})}{\tilde{\rho}_{k-1}(y_{k-1}) \mathsf{K}_k(y_{k-1}, y_k)} \\ &= \frac{\tilde{\rho}_k(y_k)}{\tilde{\rho}_{k-1}(y_{k-1})} \cdot \frac{\rho_k(y_{k-1})}{\rho_k(y_k)} = \frac{\tilde{\rho}_k(y_{k-1})}{\tilde{\rho}_{k-1}(y_{k-1})}, \end{aligned} \quad (15)$$

where we used $\rho_k = \tilde{\rho}_k/Z_k$ so that $\tilde{\rho}_k(y_k)/\rho_k(y_k) = Z_k$ and $\rho_k(y_{k-1}) = \tilde{\rho}_k(y_{k-1})/Z_k$.

B Score Test Functions

In this section, we show how we can derive control-variate schedules for minimising the variance of score estimators under different regimes. We do so for general base and target densities.

B.1 Denoising and Target Score Identities for General Base ν

To define a general score test function with a control-variate schedule, we first present lemmas that extend DSI and TSI to general base distributions.

Lemma A.1 (Denoising Score Identity for General Base ν). *For $t \in [0, 1]$, it holds that*

$$\nabla \log \mu_t(x) = \mathbb{E}_{\varrho_{t,x}} \left[\frac{1}{\sqrt{1-\lambda_t}} \nabla \log \nu \left(\frac{x - \sqrt{\lambda_t} Y}{\sqrt{1-\lambda_t}} \right) \right].$$

Proof. Recall that the diffusion path marginal μ_t is defined by the convolution

$$\mu_t(x) := \int \frac{1}{\sqrt{\lambda_t(1-\lambda_t)^d}} \nu \left(\frac{x-u}{\sqrt{1-\lambda_t}} \right) \pi \left(\frac{u}{\sqrt{\lambda_t}} \right) du.$$

With a change of variables $u = \sqrt{\lambda_t} y$, we have $du = \sqrt{\lambda_t} dy$ and

$$\mu_t(x) = \int \frac{1}{\sqrt{1-\lambda_t}^d} \nu \left(\frac{x - \sqrt{\lambda_t} y}{\sqrt{1-\lambda_t}} \right) \pi(y) dy.$$

Note that the integrand is precisely the unnormalised posterior. From here, we can solve for the score

$$\begin{aligned} \nabla \log \mu_t(x) &= \frac{\nabla \mu_t(x)}{\mu_t(x)} = \frac{1}{\mu_t(x)} \int \nabla \left(\frac{1}{\sqrt{1-\lambda_t}^d} \nu \left(\frac{x - \sqrt{\lambda_t} y}{\sqrt{1-\lambda_t}} \right) \pi(y) \right) dy \\ &= \int \left(\frac{1}{\mu_t(x)} \frac{1}{\sqrt{1-\lambda_t}^d} \nu \left(\frac{x - \sqrt{\lambda_t} y}{\sqrt{1-\lambda_t}} \right) \pi(y) \right) \frac{1}{\sqrt{1-\lambda_t}} \nabla \log \nu \left(\frac{x - \sqrt{\lambda_t} y}{\sqrt{1-\lambda_t}} \right) dy \\ &= \int \varrho_{t,x}(y) \frac{1}{\sqrt{1-\lambda_t}} \nabla \log \nu \left(\frac{x - \sqrt{\lambda_t} y}{\sqrt{1-\lambda_t}} \right) dy = \mathbb{E}_{\varrho_{t,x}} \left[\frac{1}{\sqrt{1-\lambda_t}} \nabla \log \nu \left(\frac{x - \sqrt{\lambda_t} Y}{\sqrt{1-\lambda_t}} \right) \right]. \end{aligned}$$

□

Lemma A.2 (Target Score Identity for General Base ν). *For $t \in [0, 1]$, it holds that*

$$\nabla \log \mu_t(x) = \mathbb{E}_{\varrho_{t,x}} \left[\frac{1}{\sqrt{\lambda_t}} \nabla \log \pi(Y) \right].$$

Proof. As the diffusion path marginal μ_t is a convolution, we have that

$$\mu_t(x) = \int \frac{1}{\sqrt{\lambda_t(1-\lambda_t)}^d} \nu \left(\frac{u}{\sqrt{1-\lambda_t}} \right) \pi \left(\frac{x-u}{\sqrt{\lambda_t}} \right) du.$$

Solving for the score

$$\begin{aligned} \nabla \log \mu_t(x) &= \frac{\nabla \mu_t(x)}{\mu_t(x)} = \frac{1}{\mu_t(x)} \int \nabla \left(\frac{1}{\sqrt{\lambda_t(1-\lambda_t)}^d} \nu \left(\frac{u}{\sqrt{1-\lambda_t}} \right) \pi \left(\frac{x-u}{\sqrt{\lambda_t}} \right) \right) du \\ &= \int \left(\frac{1}{\mu_t(x)} \frac{1}{\sqrt{\lambda_t(1-\lambda_t)}^d} \nu \left(\frac{u}{\sqrt{1-\lambda_t}} \right) \pi \left(\frac{x-u}{\sqrt{\lambda_t}} \right) \right) \frac{1}{\sqrt{\lambda_t}} \nabla \log \pi \left(\frac{x-u}{\sqrt{\lambda_t}} \right) du. \end{aligned}$$

Using a change of variables $u = x - \sqrt{\lambda_t}y$, we have $du = \left| -\sqrt{\lambda_t} \right| dy$ and

$$\begin{aligned} \nabla \log \mu_t(x) &= \int \left(\frac{1}{\mu_t(x)} \frac{1}{\sqrt{1-\lambda_t}^d} \nu \left(\frac{x - \sqrt{\lambda_t}y}{\sqrt{1-\lambda_t}} \right) \pi(y) \right) \frac{1}{\sqrt{\lambda_t}} \nabla \log \pi(y) dy \\ &= \int \varrho_{t,x}(y) \frac{1}{\sqrt{\lambda_t}} \nabla \log \pi(y) dy = \mathbb{E}_{\varrho_{t,x}} \left[\frac{1}{\sqrt{\lambda_t}} \nabla \log \pi(Y) \right]. \end{aligned}$$

□

Proposition A.1. *As a consequence of Lemma A.1 and Lemma A.2, for $\mathbf{A} \in \mathbb{R}^{d \times d}$ and $t \in [0, 1]$, it holds that*

$$\nabla \log \mu_t(x) = \mathbb{E}_{\varrho_{t,x}} \left[\frac{1}{\sqrt{1-\lambda_t}} \mathbf{A} \nabla \log \nu \left(\frac{x - \sqrt{\lambda_t}Y}{\sqrt{1-\lambda_t}} \right) + \frac{1}{\sqrt{\lambda_t}} (\mathbf{I} - \mathbf{A}) \nabla \log \pi(Y) \right].$$

Proof. The proof is immediate as a convex combination of the two identities given in Lemma A.1 and Lemma A.2. □

B.2 Control Variate Schedules

Remark A.1. The identity in Proposition A.1 can be viewed as introducing a matrix-valued control variate. To see this, starting from Lemma A.1 and the fact that $\mathbb{E}_{\varrho_{t,x}} [\nabla \log \varrho_{t,x}(Y)] = 0$, we can choose a control variate matrix $\mathbf{B} \in \mathbb{R}^{d \times d}$ to get

$$\begin{aligned} \nabla \log \mu_t(x) &= \mathbb{E}_{\varrho_{t,x}} \left[\frac{1}{\sqrt{1-\lambda_t}} \nabla \log \nu \left(\frac{x - \sqrt{\lambda_t}Y}{\sqrt{1-\lambda_t}} \right) - \mathbf{B} \nabla \log \varrho_{t,x}(Y) \right] + \mathbf{B}\mathbf{0} \\ &= \mathbb{E}_{\varrho_{t,x}} \left[\frac{1}{\sqrt{1-\lambda_t}} \nabla \log \nu \left(\frac{x - \sqrt{\lambda_t}Y}{\sqrt{1-\lambda_t}} \right) - \mathbf{B} \left(-\frac{\sqrt{\lambda_t}}{\sqrt{1-\lambda_t}} \nabla \log \nu \left(\frac{x - \sqrt{\lambda_t}Y}{\sqrt{1-\lambda_t}} \right) + \nabla \log \pi(Y) \right) \right] \\ &= \mathbb{E}_{\varrho_{t,x}} \left[\frac{1}{\sqrt{1-\lambda_t}} (\mathbf{I} + \sqrt{\lambda_t} \mathbf{B}) \nabla \log \nu \left(\frac{x - \sqrt{\lambda_t}Y}{\sqrt{1-\lambda_t}} \right) - \frac{1}{\sqrt{\lambda_t}} (\sqrt{\lambda_t} \mathbf{B}) \nabla \log \pi(Y) \right]. \end{aligned}$$

Denoting $\mathbf{A} := \mathbf{I} + \sqrt{\lambda_t} \mathbf{B}$, we precisely have the convex combination stated above. □

Next we start our analysis from the scalar case. Recall that $\phi_{t,x}^{\alpha \mathbf{I}}(y) = \frac{\alpha}{\sqrt{1-\lambda_t}} \nabla \log \nu \left(\frac{x - \sqrt{\lambda_t}Y}{\sqrt{1-\lambda_t}} \right) + \frac{1-\alpha}{\sqrt{\lambda_t}} \nabla \log \pi(Y)$. Having introduced a control variate, we now seek the schedule α_t minimising the variance of score estimates.

Lemma A.3. Fix $x \in \mathbb{R}^d$, the x -dependent CV schedule $\alpha_{t,x}^* \in \mathbb{R}$ minimising the variance of the score estimate is given by

$$\alpha_{t,x}^* = \operatorname{argmin}_{\alpha \in \mathbb{R}} \operatorname{Var}_{\varrho_{t,x}} [\phi_{t,x}^{\alpha \mathbf{I}}(Y)] = \frac{\mathbb{E}_{\varrho_{t,x}} [\langle \nabla \log \pi(Y), \nabla \log \varrho_{t,x}(Y) \rangle]}{\mathbb{E}_{\varrho_{t,x}} [\|\nabla \log \varrho_{t,x}(Y)\|^2]}.$$

Proof. Denote $s_1(x, y) := \frac{1}{\sqrt{1-\lambda_t}} \nabla \log \nu \left(\frac{x-\sqrt{\lambda_t}y}{\sqrt{1-\lambda_t}} \right)$ and $s_2(y) := \frac{1}{\sqrt{\lambda_t}} \nabla \log \pi(y)$. The variance is given by

$$\operatorname{Var}_{\varrho_{t,x}} [\phi_{t,x}^{\alpha \mathbf{I}}(Y)] = \mathbb{E}_{\varrho_{t,x}} [\|\alpha s_1(x, Y) + (1-\alpha)s_2(Y)\|^2] - \|\nabla \log \mu_t(x)\|^2.$$

Ignoring the additive constant, we define the objective

$$\mathcal{L}_{t,x}^{\operatorname{Var}}(\alpha) = \mathbb{E}_{\varrho_{t,x}} [\|\alpha s_1(x, Y) + (1-\alpha)s_2(Y)\|^2],$$

and want to find the minimiser $\alpha_{t,x}^* = \operatorname{argmin}_{\alpha \in \mathbb{R}} \mathcal{L}_{t,x}^{\operatorname{Var}}(\alpha)$. Rearranging the objective in terms of α , we get

$$\begin{aligned} \mathcal{L}_{t,x}^{\operatorname{Var}}(\alpha) &= \mathbb{E}_{\varrho_{t,x}} [\alpha^2 \|s_1(x, Y)\|^2 + 2\alpha(1-\alpha)\langle s_1(x, Y), s_2(Y) \rangle + (1-\alpha)^2 \|s_2(Y)\|^2] \\ &= \alpha^2 \mathbb{E}_{\varrho_{t,x}} [\|s_1(x, Y) - s_2(Y)\|^2] + \alpha \mathbb{E}_{\varrho_{t,x}} [2\langle s_2(Y), s_1(x, Y) - s_2(Y) \rangle] + \mathbb{E}_{\varrho_{t,x}} [\|s_2(Y)\|^2]. \end{aligned}$$

Taking the derivative with respect to α , we have

$$\frac{\partial}{\partial \alpha} \mathcal{L}_{t,x}^{\operatorname{Var}}(\alpha) = 2\alpha \mathbb{E}_{\varrho_{t,x}} [\|s_1(x, Y) - s_2(Y)\|^2] + 2\mathbb{E}_{\varrho_{t,x}} [\|s_2(Y), s_1(x, Y) - s_2(Y)\|^2],$$

and equating it to zero yields the stationary solution

$$\alpha_{t,x}^* = \frac{\mathbb{E}_{\varrho_{t,x}} [\langle -s_2(Y), s_1(x, Y) - s_2(Y) \rangle]}{\mathbb{E}_{\varrho_{t,x}} [\|s_1(x, Y) - s_2(Y)\|^2]}.$$

As the objective has a positive second derivative everywhere

$$\begin{aligned} \frac{\partial^2}{\partial \alpha^2} \mathcal{L}_{t,x}^{\operatorname{Var}}(\alpha) &= 2\mathbb{E}_{\varrho_{t,x}} [\|s_1(x, Y) - s_2(Y)\|^2] \\ &= 2\mathbb{E}_{\varrho_{t,x}} [\|\nabla \log \varrho_{t,x}(Y)\|^2] > 0, \end{aligned}$$

this is indeed a global minimiser. Rewriting $-s_1(x, y) + s_2(y) = \frac{1}{\sqrt{\lambda_t}} \nabla \log \varrho_{t,x}(y)$, we have

$$\alpha_{t,x}^* = \frac{\mathbb{E}_{\varrho_{t,x}} [\langle \nabla \log \pi(Y), \nabla \log \varrho_{t,x}(Y) \rangle]}{\mathbb{E}_{\varrho_{t,x}} [\|\nabla \log \varrho_{t,x}(Y)\|^2]}.$$

□

As we have auxiliary variables for estimating expectations with respect to $\varrho_{t,x}$ and evaluate the target score at their positions when propagating them, we can estimate the optimal schedule above at no additional cost. This schedule, however, is a function of x . Being mindful of estimation in practice, it may be beneficial to predict a single time-varying schedule to be used for all the samples. A natural choice is to minimise the expectation of the objective with respect to μ_t , i.e. find $\alpha_{t,x}^* = \operatorname{argmin}_{\alpha \in \mathbb{R}} \mathbb{E}_{\mu_t} [\mathcal{L}_{t,x}^{\operatorname{Var}}(\alpha)]$.

To do this, we first show a result allowing us to rewrite dot products of double expectations with respect to the path marginal and the posterior into expectations with respect to the endpoint distributions. This is made possible due to the hierarchical structure of how the samples and auxiliary variables are defined.

Lemma A.4. For sufficiently smooth test functions ϕ , we have that

$$\mathbb{E}_{\mu_t} [\mathbb{E}_{\varrho_{t,x}} [\langle \phi(Y), \nabla \log \varrho_{t,x}(Y) \rangle]] = \mathbb{E}_{\pi} [\langle \phi(X), \nabla \log \pi(X) \rangle], \quad (16)$$

$$\mathbb{E}_{\mu_t} \left[\mathbb{E}_{\varrho_{t,x}} \left[\left\langle \phi \left(\frac{X - \sqrt{\lambda_t}Y}{\sqrt{1-\lambda_t}} \right), \nabla \log \varrho_{t,x}(Y) \right\rangle \right] \right] = -\sqrt{\frac{\lambda_t}{1-\lambda_t}} \mathbb{E}_{\nu} [\langle \phi(X), \nabla \log \nu(X) \rangle]. \quad (17)$$

Proof. These results follow after invoking Stein's lemma and marginalising out a variable. We first show (16). Denote the LHS by Φ_1 . Using Stein's lemma in the inner expectation, we have

$$\Phi_1 = \mathbb{E}_{\mu_t} [\mathbb{E}_{\varrho_{t,X}} [\langle \phi(Y), \nabla \log \varrho_{t,X}(Y) \rangle]] = \mathbb{E}_{\mu_t} [\mathbb{E}_{\varrho_{t,X}} [\langle \nabla, -\phi(Y) \rangle]].$$

As the inner expression only depends on Y , we can marginalise out X as follows

$$\begin{aligned} \Phi_1 &= \iint \mu_t(x) \varrho_{t,x}(y) \langle \nabla, -\phi(y) \rangle dy dx = \iint \frac{1}{\sqrt{1-\lambda_t^d}} \nu \left(\frac{x - \sqrt{\lambda_t} y}{\sqrt{1-\lambda_t}} \right) \pi(y) \langle \nabla, -\phi(y) \rangle dx dy \\ &= \int \pi(y) \langle \nabla, -\phi(y) \rangle \int \frac{1}{\sqrt{1-\lambda_t^d}} \nu \left(\frac{x - \sqrt{\lambda_t} y}{\sqrt{1-\lambda_t}} \right) dx dy \\ &= \int \pi(y) \langle \nabla, -\phi(y) \rangle dy = \mathbb{E}_\pi [\langle \nabla, -\phi(X) \rangle]. \end{aligned}$$

Invoking Stein's lemma once more, we precisely have

$$\Phi_1 = \mathbb{E}_\pi [\langle \phi(X), \nabla \log \pi(X) \rangle].$$

For (17), denote the LHS by Φ_2 . We similarly have

$$\begin{aligned} \Phi_2 &= \mathbb{E}_{\mu_t} \left[\mathbb{E}_{\varrho_{t,X}} \left[\left\langle \phi \left(\frac{X - \sqrt{\lambda_t} Y}{\sqrt{1-\lambda_t}} \right), \nabla \log \varrho_{t,X}(Y) \right\rangle \right] \right] \\ &= \mathbb{E}_{\mu_t} \left[\mathbb{E}_{\varrho_{t,X}} \left[\left\langle \nabla, -\phi \left(\frac{X - \sqrt{\lambda_t} Y}{\sqrt{1-\lambda_t}} \right) \right\rangle \right] \right] \\ &= \iint \mu_t(x) \varrho_{t,x}(y) \left\langle \nabla, -\phi \left(\frac{x - \sqrt{\lambda_t} y}{\sqrt{1-\lambda_t}} \right) \right\rangle dy dx \\ &= \iint \frac{1}{\sqrt{1-\lambda_t^d}} \nu \left(\frac{x - \sqrt{\lambda_t} y}{\sqrt{1-\lambda_t}} \right) \pi(y) \left\langle \nabla, -\phi \left(\frac{x - \sqrt{\lambda_t} y}{\sqrt{1-\lambda_t}} \right) \right\rangle dy dx. \end{aligned}$$

By a change of variables $y = \frac{1}{\sqrt{\lambda_t}}(x - \sqrt{1-\lambda_t}u)$, we have $dy = \sqrt{\frac{1-\lambda_t}{\lambda_t}} du$ and, for any divergence, $\langle \nabla_y, f(y) \rangle = -\sqrt{\frac{\lambda_t}{1-\lambda_t}} \langle \nabla_u, f \left(\frac{1}{\sqrt{\lambda_t}}(x - \sqrt{1-\lambda_t}u) \right) \rangle$. This results in

$$\begin{aligned} \Phi_2 &= \iint \nu(u) \pi \left(\frac{x - \sqrt{1-\lambda_t}u}{\sqrt{\lambda_t}} \right) \left(-\sqrt{\frac{\lambda_t}{1-\lambda_t}} \right) \langle \nabla, -\phi(u) \rangle \frac{1}{\sqrt{\lambda_t^d}} du dx \\ &= -\sqrt{\frac{\lambda_t}{1-\lambda_t}} \int \nu(u) \langle \nabla, -\phi(u) \rangle \int \frac{1}{\sqrt{\lambda_t^d}} \pi \left(\frac{x - \sqrt{1-\lambda_t}u}{\sqrt{\lambda_t}} \right) dx du \\ &= -\sqrt{\frac{\lambda_t}{1-\lambda_t}} \int \nu(u) \langle \nabla, -\phi(u) \rangle du = \sqrt{\frac{\lambda_t}{1-\lambda_t}} \mathbb{E}_\nu [\langle \nabla, \phi(X) \rangle]. \end{aligned}$$

Using Stein's lemma, we finally have

$$\Phi_2 = -\sqrt{\frac{\lambda_t}{1-\lambda_t}} \mathbb{E}_\nu [\langle \phi(X), \nabla \log \nu(X) \rangle].$$

□

Now, we minimise the variance in expectation, resulting in a position-independent schedule. It turns out to admit a simpler form, revealing a clear dependence on the endpoint distributions as well as the schedule λ_t .

B.2.1 Optimal Scalar CV Schedule

We restate the proposition for clarity and provide its proof.

Proposition 2. The scalar CV schedule $\alpha_t^* \in \mathbb{R}$ minimising the expected variance is given by

$$\alpha_t^* = \operatorname{argmin}_{\alpha \in \mathbb{R}} \mathbb{E}_{X \sim \mu_t} [\operatorname{Var}_{Y \sim \varrho_{t,X}} [\phi_{t,X}^{\alpha \mathbf{I}}(Y)]] = \frac{\frac{1}{\lambda_t} \operatorname{Var}_{\pi} [\nabla \log \pi(X)]}{\frac{1}{1-\lambda_t} \operatorname{Var}_{\nu} [\nabla \log \nu(X)] + \frac{1}{\lambda_t} \operatorname{Var}_{\pi} [\nabla \log \pi(X)]},$$

where we write $\operatorname{Var}_p[f(X)] = \operatorname{Tr}(\operatorname{Cov}_p[f(X)])$.

Proof. Denote again $s_1(x, y) := \frac{1}{\sqrt{1-\lambda_t}} \nabla \log \nu \left(\frac{x - \sqrt{\lambda_t} y}{\sqrt{1-\lambda_t}} \right)$ and $s_2(y) := \frac{1}{\sqrt{\lambda_t}} \nabla \log \pi(y)$. Similar to Lemma A.3, we can define the objective

$$\mathcal{L}_{t,x}^{\operatorname{Var}}(\alpha) = \mathbb{E}_{\varrho_{t,x}} [\|\alpha s_1(x, Y) + (1-\alpha)s_2(Y)\|^2].$$

Furthermore, we can follow the workings in Lemma A.3 to identically minimise this objective in expectation and yield

$$\alpha_t^* = \operatorname{argmin}_{\alpha \in \mathbb{R}} \mathbb{E}_{\mu_t} [\mathcal{L}_{t,X}^{\operatorname{Var}}(\alpha)] = \frac{\mathbb{E}_{\mu_t} [\mathbb{E}_{\varrho_{t,X}} [\langle \nabla \log \pi(Y), \nabla \log \varrho_{t,X}(Y) \rangle]]}{\mathbb{E}_{\mu_t} [\mathbb{E}_{\varrho_{t,X}} [\|\nabla \log \varrho_{t,X}(Y)\|^2]]}.$$

Using the results from Lemma A.4, for test functions $\phi_1(y) = \nabla \log \pi(y)$ and $\phi_2(y) = \sqrt{\frac{\lambda_t}{1-\lambda_t}} \nabla \log \nu(y)$, we have that

$$\begin{aligned} \mathbb{E}_{\mu_t} [\mathbb{E}_{\varrho_{t,X}} [\langle \phi_1(Y), \nabla \log \varrho_{t,X}(Y) \rangle]] &= \mathbb{E}_{\pi} [\langle \phi_1(X), \nabla \log \pi(X) \rangle] \\ &= \mathbb{E}_{\pi} [\|\nabla \log \pi(X)\|^2], \\ \mathbb{E}_{\mu_t} [\mathbb{E}_{\varrho_{t,X}} [\left\langle \phi_2 \left(\frac{X - \sqrt{\lambda_t} Y}{\sqrt{1-\lambda_t}} \right), \nabla \log \varrho_{t,X}(Y) \right\rangle]] &= -\sqrt{\frac{\lambda_t}{1-\lambda_t}} \mathbb{E}_{\nu} [\langle \phi(X), \nabla \log \nu(X) \rangle] \\ &= -\frac{\lambda_t}{1-\lambda_t} \mathbb{E}_{\nu} [\|\nabla \log \nu(X)\|^2]. \end{aligned}$$

Since $\nabla \log \varrho_{t,x}(y) = -\phi_2 \left(\frac{x - \sqrt{\lambda_t} y}{\sqrt{1-\lambda_t}} \right) + \phi_1(y)$, it immediately follows that

$$\alpha_t^* = \frac{\mathbb{E}_{\pi} [\|\nabla \log \pi(X)\|^2]}{\frac{\lambda_t}{1-\lambda_t} \mathbb{E}_{\nu} [\|\nabla \log \nu(X)\|^2] + \mathbb{E}_{\pi} [\|\nabla \log \pi(X)\|^2]}.$$

Rewriting to reflect the structure of the path and noting $\operatorname{Var}_p[\nabla \log p(X)] = \mathbb{E}_p [\|\nabla \log p(X)\|^2]$, we have

$$\alpha_t^* = \frac{\frac{1}{\lambda_t} \operatorname{Var}_{\pi} [\nabla \log \pi(X)]}{\frac{1}{1-\lambda_t} \operatorname{Var}_{\nu} [\nabla \log \nu(X)] + \frac{1}{\lambda_t} \operatorname{Var} [\nabla \log \pi(X)]}.$$

□

A key advantage of estimating such a schedule is we can combine all our auxiliary variables across several samples to yield a larger sample size and a more stable schedule altogether. In practice, we can use the empirical distribution formed by our propagated samples in place of μ_t .

B.2.2 Optimal Diagonal CV Schedule

Now, we consider schedules that are restricted to be diagonal. We have the following result that describes a similar optimum.

Proposition A.2. The diagonal CV schedule $\mathbf{a}_t^* = (a_{t,1}^*, \dots, a_{t,d}^*)^\top \in \mathbb{R}^d$, minimising the total variance in expectation, i.e.

$$\mathbf{a}_t^* = \operatorname{argmin}_{\mathbf{a} \in \mathbb{R}^d} \mathbb{E}_{X \sim \mu_t} [\operatorname{Var}_{Y \sim \varrho_{t,X}} [\phi_{t,X}^{\operatorname{diag}(\mathbf{a})}(Y)]],$$

has its i th component equal to

$$a_{t,i}^* = \frac{\frac{1}{\lambda_t} \mathbb{E}_{\pi} [(\nabla \log \pi(X))_i^2]}{\frac{1}{1-\lambda_t} \mathbb{E}_{\nu} [(\nabla \log \nu(X))_i^2] + \frac{1}{\lambda_t} \mathbb{E}_{\pi} [(\nabla \log \pi(X))_i^2]}.$$

Proof. Take $\mathbf{a} = (a_1, \dots, a_d)^\top \in \mathbb{R}^d$. Denote again $s_1(x, y) := \frac{1}{\sqrt{1-\lambda_t}} \nabla \log \nu \left(\frac{x-\sqrt{\lambda_t}y}{\sqrt{1-\lambda_t}} \right)$ and $s_2(y) := \frac{1}{\sqrt{\lambda_t}} \nabla \log \pi(y)$. Let us further denote the following, whose double expectation is equivalent to the variance objective up to an additive constant

$$\mathcal{L}_t^{\text{Norm}}(x, y, \mathbf{A}) := \|\phi_{t,x}^{\mathbf{A}}(y)\|^2 = \|\mathbf{A}s_1(x, y) + (\mathbf{I} - \mathbf{A})s_2(y)\|^2.$$

Using the fact \mathbf{A} is diagonal, we can rewrite it to decouple the contributions of the diagonal components

$$\mathcal{L}_t^{\text{Norm}}(x, y, \text{diag}(\mathbf{a})) = \sum_{i=1}^d [a_i s_1^i(x, y) + (1 - a_i) s_2^i(y)]^2,$$

where s_1^i and s_2^i are the i th components of s_1 and s_2 . Solving for a stationary solution to the original objective, we take the partial derivatives component-wise and move them inside the expectation, i.e. for the i th component,

$$\begin{aligned} & \frac{\partial}{\partial a_i} \mathbb{E}_{\mu_t} [\mathbb{E}_{\varrho_{t,X}} [\mathcal{L}_t^{\text{Norm}}(X, Y, \text{diag}(\mathbf{a}))]] \\ &= \mathbb{E}_{\mu_t} [\mathbb{E}_{\varrho_{t,X}} [2 [a_i s_1^i(X, Y) + (1 - a_i) s_2^i(Y)] (s_1^i(X, Y) - s_2^i(Y))]] \\ &= 2a_i \mathbb{E}_{\mu_t} [\mathbb{E}_{\varrho_{t,X}} [(s_1^i(X, Y) - s_2^i(Y))^2]] + 2\mathbb{E}_{\mu_t} [\mathbb{E}_{\varrho_{t,X}} [s_2^i(Y) (s_1^i(X, Y) - s_2^i(Y))]]. \end{aligned}$$

Setting this to zero, we arrive at the stationary solution

$$a_{t,i}^* = \frac{\mathbb{E}_{\mu_t} [\mathbb{E}_{\varrho_{t,X}} [-s_2^i(Y) (s_1^i(X, Y) - s_2^i(Y))]]}{\mathbb{E}_{\mu_t} [\mathbb{E}_{\varrho_{t,X}} [(s_1^i(X, Y) - s_2^i(Y))^2]]}.$$

Define for now $\phi_1(u) = \frac{1}{\sqrt{1-\lambda_t}} (\nabla \log \nu(u))_i \mathbf{e}_i$, so we have $\phi_1 \left(\frac{x-\sqrt{\lambda_t}y}{\sqrt{1-\lambda_t}} \right) = s_1^i(x, y) \mathbf{e}_i$. Define also $\phi_2(u) = \frac{1}{\sqrt{\lambda_t}} (\nabla \log \pi(u))_i \mathbf{e}_i = s_2^i(u) \mathbf{e}_i$. Using the fact that $s_1(x, y) - s_2(y) = -\frac{1}{\sqrt{\lambda_t}} \nabla \log \varrho_{t,X}(y)$ and invoking Lemma A.4 for test functions ϕ_1 and ϕ_2 , we have that

$$\begin{aligned} \mathbb{E}_{\mu_t} [\mathbb{E}_{\varrho_{t,X}} [s_1^i(X, Y) (s_1^i(X, Y) - s_2^i(Y))]] &= \mathbb{E}_{\mu_t} [\mathbb{E}_{\varrho_{t,X}} [\langle s_1^i(X, Y) \mathbf{e}_i, s_1(X, Y) - s_2(Y) \rangle]] \\ &= -\frac{1}{\sqrt{\lambda_t}} \mathbb{E}_{\mu_t} \left[\mathbb{E}_{\varrho_{t,X}} \left[\left\langle \phi_1 \left(\frac{X-\sqrt{\lambda_t}Y}{\sqrt{1-\lambda_t}} \right), \nabla \log \varrho_{t,X}(Y) \right\rangle \right] \right] \\ &= \frac{1}{\sqrt{\lambda_t}} \sqrt{\frac{\lambda_t}{1-\lambda_t}} \mathbb{E}_\nu [\langle \phi_1(X), \nabla \log \nu(X) \rangle] = \frac{1}{1-\lambda_t} \mathbb{E}_\nu [(\nabla \log \nu(X))_i^2], \\ \mathbb{E}_{\mu_t} [\mathbb{E}_{\varrho_{t,X}} [s_2^i(Y) (s_1^i(X, Y) - s_2^i(Y))]] &= \mathbb{E}_{\mu_t} [\mathbb{E}_{\varrho_{t,X}} [\langle s_2^i(Y) \mathbf{e}_i, s_1(X, Y) - s_2(Y) \rangle]] \\ &= -\frac{1}{\sqrt{\lambda_t}} \mathbb{E}_{\mu_t} [\mathbb{E}_{\varrho_{t,X}} [\langle \phi_2(Y), \nabla \log \varrho_{t,X}(Y) \rangle]] \\ &= -\frac{1}{\sqrt{\lambda_t}} \mathbb{E}_\pi [\langle \phi_2(X), \nabla \log \pi(X) \rangle] = -\frac{1}{\lambda_t} \mathbb{E}_\pi [(\nabla \log \pi(X))_i^2]. \end{aligned}$$

Hence the i th component of this stationary solution is given by

$$a_{t,i}^* = \frac{\frac{1}{\lambda_t} \mathbb{E}_\pi [(\nabla \log \pi(X))_i^2]}{\frac{1}{1-\lambda_t} \mathbb{E}_\nu [(\nabla \log \nu(X))_i^2] + \frac{1}{\lambda_t} \mathbb{E}_\pi [(\nabla \log \pi(X))_i^2]}.$$

Inspecting the second-order partial derivatives, we have that

$$\begin{aligned} & \frac{\partial^2}{\partial a_i^2} \mathbb{E}_{\mu_t} [\mathbb{E}_{\varrho_{t,X}} [\mathcal{L}_t^{\text{Norm}}(X, Y, \text{diag}(\mathbf{a}))]] \\ &= 2\mathbb{E}_{\mu_t} [\mathbb{E}_{\varrho_{t,X}} [(s_1^i(X, Y) - s_2^i(Y))^2]] \\ &= \frac{2}{1-\lambda_t} \mathbb{E}_\nu [(\nabla \log \nu(X))_i^2] + \frac{2}{\lambda_t} \mathbb{E}_\pi [(\nabla \log \pi(X))_i^2] > 0, \end{aligned}$$

and $\frac{\partial^2}{\partial a_i \partial a_j} \mathbb{E}_{\mu_t} [\mathbb{E}_{\varrho_{t,X}} [\mathcal{L}_t^{\text{Norm}}(X, Y, \text{diag}(\mathbf{a}))]] = 0$ for $i \neq j$ for all $\mathbf{a} \in \mathbb{R}^d$. Hence, the Hessian is positive definite everywhere, given that it is diagonal with positive eigenvalues. We can conclude that the objective is convex and the stationary solution $a_{t,x}^*$ is indeed a global minimiser. \square

B.2.3 Optimal Matrix CV Schedule

Now, we consider arbitrary matrix schedules. We restate the proposition and provide its proof.

Proposition 3. *The matrix CV schedule $\mathbf{A}_t^* \in \mathbb{R}^{d \times d}$ minimising the expected variance is given by*

$$\mathbf{A}_t^* = \underset{\mathbf{A} \in \mathbb{R}^{d \times d}}{\operatorname{argmin}} \mathbb{E}_{X \sim \mu_t} [\operatorname{Var}_{Y \sim \varrho_{t,X}} [\phi_{t,X}^{\mathbf{A}}(Y)]] = \frac{1}{\lambda_t} \mathcal{I}_{\pi} \left(\frac{1}{1 - \lambda_t} \mathcal{I}_{\nu} + \frac{1}{\lambda_t} \mathcal{I}_{\pi} \right)^{-1},$$

where \mathcal{I}_p denotes the covariance of the score of p , i.e.

$$\mathcal{I}_p := \operatorname{Cov}_p [\nabla \log p(X)] = \mathbb{E}_p [\nabla \log p(X) \nabla \log p(X)^T].$$

Proof. Take $\mathbf{A} \in \mathbb{R}^{d \times d}$ and refer to A_{ij} as its (i, j) entry. Denote again $s_1(x, y) := \frac{1}{\sqrt{1 - \lambda_t}} \nabla \log \nu \left(\frac{x - \sqrt{\lambda_t} y}{\sqrt{1 - \lambda_t}} \right)$ and $s_2(y) := \frac{1}{\sqrt{\lambda_t}} \nabla \log \pi(y)$. Let us refer to the following, whose double expectation is equivalent to the variance objective up to an additive constant

$$\mathcal{L}_t^{\text{Norm}}(x, y, \mathbf{A}) := \|\phi_{t,x}^{\mathbf{A}}(y)\|^2 = \|\mathbf{A}s_1(x, y) + (\mathbf{I} - \mathbf{A})s_2(y)\|^2.$$

We can rewrite it as follows to show the contributions of the individual entries of the matrix

$$\begin{aligned} \mathcal{L}_t^{\text{Norm}}(x, y, \mathbf{A}) &= \sum_{l=1}^d (s_2(y) + \mathbf{A}(s_1(x, y) - s_2(y)))_l^2 \\ &= \sum_{l=1}^d \left(s_2^l(y) + \sum_{k=1}^d A_{lk} (s_1^k(x, y) - s_2^k(y)) \right)^2, \end{aligned}$$

where s_1^i and s_2^i are the i th components of s_1 and s_2 . Taking the derivative with respect to A_{ij} , we have

$$\begin{aligned} \frac{\partial}{\partial A_{ij}} \mathcal{L}_t^{\text{Norm}}(x, y, \mathbf{A}) &= 2 \left(s_2^i(y) + \sum_{k=1}^d A_{ik} (s_1^k(x, y) - s_2^k(y)) \right) (s_1^j(x, y) - s_2^j(y)) \\ &= 2s_2^i(y)(s_1^j(x, y) - s_2^j(y)) + 2 \sum_{k=1}^d A_{ik} (s_1^k(x, y) - s_2^k(y))(s_1^j(x, y) - s_2^j(y)). \end{aligned}$$

Now, we can consider the actual objective and take the derivative with respect to A_{ij}

$$\begin{aligned} &\frac{\partial}{\partial A_{ij}} \mathbb{E}_{\mu_t} [\mathbb{E}_{\varrho_{t,X}} [\mathcal{L}_t^{\text{Norm}}(X, Y, \mathbf{A})]] \\ &= \mathbb{E}_{\mu_t} \left[\mathbb{E}_{\varrho_{t,X}} \left[\frac{\partial}{\partial A_{ij}} \mathcal{L}_t^{\text{Norm}}(X, Y, \mathbf{A}) \right] \right] \\ &= 2\mathbb{E}_{\mu_t} [\mathbb{E}_{\varrho_{t,X}} [s_2^i(Y)(s_1^j(X, Y) - s_2^j(Y))]] + 2 \sum_{k=1}^d A_{ik} \mathbb{E}_{\mu_t} [\mathbb{E}_{\varrho_{t,X}} [s_1^k(X, Y) - s_2^k(Y)] (s_1^j(X, Y) - s_2^j(Y))]. \end{aligned}$$

Define $\phi_1(u) = \frac{1}{\sqrt{1 - \lambda_t}} (\nabla \log \nu(u))_i \mathbf{e}_j$, so we have $\phi_1 \left(\frac{x - \sqrt{\lambda_t} y}{\sqrt{1 - \lambda_t}} \right) = s_1^i(x, y) \mathbf{e}_j$, and also $\phi_2(u) = \frac{1}{\sqrt{\lambda_t}} (\nabla \log \pi(u))_i \mathbf{e}_j = s_2^i(u) \mathbf{e}_j$. Using the fact that $s_1(x, y) - s_2(y) = -\frac{1}{\sqrt{\lambda_t}} \nabla \log \varrho_{t,X}(y)$ and invoking Lemma A.4 for test functions ϕ_1 and ϕ_2 , we have that

$$\begin{aligned} &\mathbb{E}_{\mu_t} [\mathbb{E}_{\varrho_{t,X}} [s_1^i(X, Y)(s_1^j(X, Y) - s_2^j(Y))]] && \mathbb{E}_{\mu_t} [\mathbb{E}_{\varrho_{t,X}} [s_2^i(Y)(s_1^j(X, Y) - s_2^j(Y))]] \\ &= \mathbb{E}_{\mu_t} [\mathbb{E}_{\varrho_{t,X}} [\langle s_1^i(X, Y) \mathbf{e}_j, s_1(X, Y) - s_2(Y) \rangle]] && = \mathbb{E}_{\mu_t} [\mathbb{E}_{\varrho_{t,X}} [\langle s_2^i(Y) \mathbf{e}_j, s_1(X, Y) - s_2(Y) \rangle]] \\ &= -\frac{1}{\sqrt{\lambda_t}} \mathbb{E}_{\mu_t} \left[\mathbb{E}_{\varrho_{t,X}} \left[\langle \phi_1 \left(\frac{X - \sqrt{\lambda_t} Y}{\sqrt{1 - \lambda_t}} \right), \nabla \log \varrho_{t,X}(Y) \rangle \right] \right] && = -\frac{1}{\sqrt{\lambda_t}} \mathbb{E}_{\mu_t} [\mathbb{E}_{\varrho_{t,X}} [\langle \phi_2(Y), \nabla \log \varrho_{t,X}(Y) \rangle]] \\ &= \frac{1}{\sqrt{\lambda_t}} \sqrt{\frac{\lambda_t}{1 - \lambda_t}} \mathbb{E}_{\nu} [\langle \phi_1(X), \nabla \log \nu(X) \rangle] && = -\frac{1}{\sqrt{\lambda_t}} \mathbb{E}_{\pi} [\langle \phi_2(X), \nabla \log \pi(X) \rangle] \\ &= \frac{1}{1 - \lambda_t} \mathbb{E}_{\nu} [(\nabla \log \nu(X))_i (\nabla \log \nu(X))_j], && = -\frac{1}{\lambda_t} \mathbb{E}_{\pi} [(\nabla \log \pi(X))_i (\nabla \log \pi(X))_j]. \end{aligned}$$

Note that we can rewrite

$$\mathbb{E}_p[(\nabla \log p(X))_i (\nabla \log p(X))_j] = (\mathbb{E}_p[\nabla \log p(X) \nabla \log p(X)^\top])_{ij} = (\mathcal{I}_p)_{ij},$$

and we have the simplified equalities

$$\begin{aligned}\mathbb{E}_{\mu_t}[\mathbb{E}_{\varrho_{t,X}}[s_1^i(X, Y)(s_2^j(X, Y) - s_2^j(Y))]] &= \frac{1}{1 - \lambda_t}(\mathcal{I}_\nu)_{ij}, \\ \mathbb{E}_{\mu_t}[\mathbb{E}_{\varrho_{t,X}}[s_2^i(Y)(s_1^j(X, Y) - s_1^j(Y))]] &= -\frac{1}{\lambda_t}(\mathcal{I}_\pi)_{ij}.\end{aligned}$$

We therefore have

$$\begin{aligned}\frac{\partial}{\partial A_{ij}}\mathbb{E}_{\mu_t}[\mathbb{E}_{\varrho_{t,X}}[\mathcal{L}_t^{\text{Norm}}(X, Y, \mathbf{A})]] &= -\frac{2}{\lambda_t}(\mathcal{I}_\pi)_{ij} + 2 \sum_{k=1}^d A_{ik} \left(\frac{1}{1 - \lambda_t}(\mathcal{I}_\nu)_{kj} + \frac{1}{\lambda_t}(\mathcal{I}_\pi)_{kj} \right) \\ &= -\frac{2}{\lambda_t}(\mathcal{I}_\pi)_{ij} + 2 \left(\mathbf{A} \left(\frac{1}{1 - \lambda_t} \mathcal{I}_\nu + \frac{1}{\lambda_t} \mathcal{I}_\pi \right) \right)_{ij}.\end{aligned}$$

Setting this to zero, the stationary solution must satisfy

$$\left(\mathbf{A}_t^* \left(\frac{1}{1 - \lambda_t} \mathcal{I}_\nu + \frac{1}{\lambda_t} \mathcal{I}_\pi \right) \right)_{ij} = \left(\frac{1}{\lambda_t} \mathcal{I}_\pi \right)_{ij}.$$

Since this holds for all entries (i, j) , we therefore have that

$$\mathbf{A}_t^* \left(\frac{1}{1 - \lambda_t} \mathcal{I}_\nu + \frac{1}{\lambda_t} \mathcal{I}_\pi \right) = \frac{1}{\lambda_t} \mathcal{I}_\pi \iff \mathbf{A}_t^* = \frac{1}{\lambda_t} \mathcal{I}_\pi \left(\frac{1}{1 - \lambda_t} \mathcal{I}_\nu + \frac{1}{\lambda_t} \mathcal{I}_\pi \right)^{-1}. \quad (18)$$

Inspecting the second-order partial derivatives, we have

$$\begin{aligned}\frac{\partial^2}{\partial A_{ij} \partial A_{ik}} \mathbb{E}_{\mu_t}[\mathbb{E}_{\varrho_{t,X}}[\mathcal{L}_t^{\text{Norm}}(X, Y, \mathbf{A})]] &= 2 \mathbb{E}_{\mu_t}[\mathbb{E}_{\varrho_{t,X}}[s_1^k(X, Y) - s_2^k(Y)](s_1^j(X, Y) - s_2^j(Y))] \\ &= \frac{2}{1 - \lambda_t}(\mathcal{I}_\nu)_{kj} + \frac{2}{\lambda_t}(\mathcal{I}_\pi)_{kj} = 2 \left(\frac{1}{1 - \lambda_t} \mathcal{I}_\nu + \frac{1}{\lambda_t} \mathcal{I}_\pi \right)_{kj},\end{aligned}$$

and $\frac{\partial^2}{\partial A_{ij} \partial A_{lk}} \mathbb{E}_{\mu_t}[\mathbb{E}_{\varrho_{t,X}}[\mathcal{L}_t^{\text{Norm}}(X, Y, \mathbf{A})]] = 0$ when $i \neq l$. Let us denote by $\mathbf{a} = (a_1, \dots, a_{d^2})^\top \in \mathbb{R}^{d^2}$, the flattened representation of \mathbf{A} , with $a_{d(i-1)+j} = A_{ij}$. It follows then that our Hessian is a block diagonal matrix

$$\mathbf{H}(\mathbf{a}) = \left(\frac{\partial^2 \mathbb{E}_{\mu_t}[\mathbb{E}_{\varrho_{t,X}}[\mathcal{L}_t^{\text{Norm}}(X, Y, \mathbf{A})]]}{\partial a_i \partial a_j} \right) = \begin{bmatrix} \tilde{\mathbf{H}} & 0 & 0 & 0 \\ 0 & \tilde{\mathbf{H}} & 0 & 0 \\ 0 & 0 & \ddots & 0 \\ 0 & 0 & 0 & \tilde{\mathbf{H}} \end{bmatrix},$$

where the identical blocks are given by

$$\tilde{\mathbf{H}} = \frac{2}{1 - \lambda_t} \mathcal{I}_\nu + \frac{2}{\lambda_t} \mathcal{I}_\pi.$$

As the score covariances are positive definite, their linear combination in $\tilde{\mathbf{H}}$ is also positive definite and has positive eigenvalues. The block diagonal $\mathbf{H}(\mathbf{a})$ inherits the eigenvalues of its blocks, which are all positive, and hence the Hessian is positive definite everywhere. We can conclude that our objective is convex and the stationary solution \mathbf{A}_t^* is indeed the global minimiser. \square

C Diffusion Path Design

In this section, we point out the biasedness of DALD and how we can use this to inform our choice for the λ_t schedule.

C.1 Diffusion Annealed Langevin Dynamics

It is worth noting that, even when diffusion annealed Langevin dynamics (4) is simulated without discretisation error, it remains biased, since the marginal distributions of the solution to the corresponding SDE do not exactly coincide with $\mu_{t/T}$, in contrast to the stochastic interpolants formulation proposed by Albergo et al. [2025]. However, this bias can be quantified. In particular, bounds have been established in Guo et al. [2024, Theorem 1] and Cordero-Encinar et al. [2025a, Theorem A.3]. We state the result below.

Theorem A.1. *Let $\mathbb{P}_{\text{DALD}} = (p_{t,\text{DALD}})_{t \in [0,T]}$ be the path measure of the diffusion annealed Langevin dynamics (4), and $\mathbb{P} = (\hat{\mu}_t)_{t \in [0,T]}$ that of a reference SDE such that the marginals at each time have distribution $\mu_{t/T}$. If $p_{0,\text{DALD}} = \hat{\mu}_0$, the KL divergence between the path measures is given by*

$$\text{KL}(\hat{\mu}_T \| p_{T,\text{DALD}}) \leq \text{KL}(\mathbb{P} \| \mathbb{P}_{\text{DALD}}) = \frac{1}{4T} \mathcal{A}(\mu).$$

The proof follows from an application of Girsanov's theorem [Karatzas and Shreve, 1991], we refer to the aforementioned works for details. Following Cordero-Encinar et al. [2025a, Lemma 3.3], we can obtain an upper bound for the action of the diffusion path (1). We outline the details below.

First, consider the reparametrised version of μ_t in terms of the schedule λ_t , denoted as $\tilde{\mu}_\lambda$ and let $X_\lambda \sim \tilde{\mu}_\lambda$ and $X_{\lambda+\delta} \sim \tilde{\mu}_{\lambda+\delta}$. Recall that

$$X_\lambda = \sqrt{\lambda}X + \sqrt{1-\lambda}\sigma Z \quad (19)$$

where $X \sim \pi$ and $Z \sim \mathcal{N}(0, I)$ are independent random variables. The Wasserstein-2 distance between $\tilde{\mu}_\lambda$ and $\tilde{\mu}_{\lambda+\delta}$ is given by

$$\begin{aligned} W_2^2(\tilde{\mu}_\lambda, \tilde{\mu}_{\lambda+\delta}) &\leq \mathbb{E} [\|X_\lambda - X_{\lambda+\delta}\|^2] \\ &= \mathbb{E} \left[\left\| (\sqrt{\lambda} - \sqrt{\lambda+\delta})X + \sqrt{1-\lambda} - \sqrt{1-\lambda-\delta} \right\|^2 \right] + \mathbb{E} \left[\left\| (\sqrt{1-\lambda} - \sqrt{1-\lambda-\delta})\sigma Z \right\|^2 \right] \\ &= (\sqrt{\lambda} - \sqrt{\lambda+\delta})^2 \mathbb{E} [\|X\|^2] + (\sqrt{1-\lambda} - \sqrt{1-\lambda-\delta})^2 \sigma^2 d. \end{aligned}$$

Using the definition of the metric derivative we have

$$|\dot{\tilde{\mu}}|_\lambda^2 = \lim_{\delta \rightarrow 0} \frac{W_2^2(\tilde{\mu}_\lambda, \tilde{\mu}_{\lambda+\delta})}{\delta^2} \leq \frac{\mathbb{E} [\|X\|^2]}{4\lambda} + \frac{\sigma^2 d}{4(1-\lambda)}.$$

Therefore, we have the following expression for the action

$$\begin{aligned} \mathcal{A}_\lambda(\mu) &= \int_0^1 |\dot{\tilde{\mu}}|_t^2 dt = \int_0^1 |\dot{\tilde{\mu}}|_\lambda^2 |\partial_t \lambda_t|^2 dt \\ &\leq \int_0^1 \left(\frac{\mathbb{E} [\|X\|^2]}{4\lambda_t} + \frac{\sigma^2 d}{4(1-\lambda_t)} \right) |\partial_t \lambda_t|^2 dt \end{aligned}$$

This expression will be used later to derive a principled schedule λ_t that minimises this upper bound.

C.2 Schedule Minimising Action Upper Bound

We want to find the curve $\lambda = (\lambda_t)_{t \in [0,1]}$ that minimises the upper bound of the action functional. In Theorem A.1, we were able to bound the action by a simpler functional. The following result indicates its minimiser.

Proposition A.3. *The cosine schedule $\lambda_t = \sin^2(\frac{\pi t}{2})$ is the unique minimiser of the functional*

$$J[\lambda] = \int_0^1 \left(\frac{\sigma^2 d}{4(1-\lambda_t)} + \frac{\mathbb{E}_\pi [\|X\|^2]}{4\lambda_t} \right) (\partial_t \lambda_t)^2 dt.$$

Proof. Denote $\dot{\lambda}_t = \partial_t \lambda_t$ as the time derivative of the schedule and define the Lagrangian as

$$L(t, \lambda_t, \dot{\lambda}_t) = \dot{\lambda}_t^2 \left(\frac{\sigma^2 d}{4(1 - \lambda_t)} + \frac{\mathbb{E}_\pi[\|X\|^2]}{4\lambda_t} \right),$$

then any stationary points of the functional $J[\lambda] = \int_0^1 L(t, \lambda_t, \dot{\lambda}_t) dt$ must satisfy the Euler-Lagrange equation

$$\frac{\partial L}{\partial \lambda_t} - \frac{d}{dt} \frac{\partial L}{\partial \dot{\lambda}_t} = 0.$$

We drop the time index in writing λ and $\dot{\lambda}$ for conciseness. We have that

$$\begin{aligned} \frac{\partial L}{\partial \lambda} &= \dot{\lambda}^2 \left(-\frac{\mathbb{E}_\pi[\|X\|^2]}{4\lambda^2} + \frac{\sigma^2 d}{4(1 - \lambda)^2} \right) \\ -\frac{d}{dt} \frac{\partial L}{\partial \dot{\lambda}} &= -\frac{d}{dt} \left(2\dot{\lambda} \left(\frac{\mathbb{E}_\pi[\|X\|^2]}{4\lambda} + \frac{\sigma^2 d}{4(1 - \lambda)} \right) \right) \\ &= -2\ddot{\lambda} \left(\frac{\mathbb{E}_\pi[\|X\|^2]}{4\lambda} + \frac{\sigma^2 d}{4(1 - \lambda)} \right) - 2\dot{\lambda}^2 \left(-\frac{\mathbb{E}_\pi[\|X\|^2]}{4\lambda^2} + \frac{\sigma^2 d}{4(1 - \lambda)^2} \right). \end{aligned}$$

Equating their sum to zero, we can solve for $\ddot{\lambda}$

$$\begin{aligned} \ddot{\lambda} &= -\frac{1}{2} \dot{\lambda}^2 \frac{-\frac{\mathbb{E}_\pi[\|X\|^2]}{4\lambda^2} + \frac{\sigma^2 d}{4(1 - \lambda)^2}}{\frac{\mathbb{E}_\pi[\|X\|^2]}{4\lambda} + \frac{\sigma^2 d}{4(1 - \lambda)}} \\ &= \frac{1}{2} \dot{\lambda}^2 \frac{(1 - \lambda)^2 \mathbb{E}_\pi[\|X\|^2] - \lambda^2 \sigma^2 d}{\lambda(1 - \lambda)^2 \mathbb{E}_\pi[\|X\|^2] + \lambda^2(1 - \lambda)\sigma^2 d}. \end{aligned}$$

We denote the ratio $\sigma^2 d / \mathbb{E}_\pi[\|X\|^2] =: R$ and rewrite the above as

$$\ddot{\lambda} = \frac{1}{2} \dot{\lambda}^2 \frac{(1 - \lambda)^2 - R\lambda^2}{\lambda(1 - \lambda)^2 + R\lambda^2(1 - \lambda)},$$

As there are no t terms, we can use the substitution $\dot{\lambda} = v(\lambda)$, which yields $\ddot{\lambda} = \dot{v}v$. We have

$$\dot{v}(\lambda)v(\lambda) = \frac{1}{2}v(\lambda)^2 \frac{(1 - \lambda)^2 - R\lambda^2}{\lambda(1 - \lambda)^2 + R\lambda^2(1 - \lambda)},$$

and rearranging reveals a first-order differential equation

$$\dot{v}(\lambda) + v(\lambda) \underbrace{\left[-\frac{(1 - \lambda)^2 - R\lambda^2}{2\lambda(1 - \lambda)^2 + 2R\lambda^2(1 - \lambda)} \right]}_{p(\lambda)} = 0.$$

which we can solve using an integrating factor

$$\begin{aligned} I(\lambda) &= \exp \left(\int p(\lambda) d\lambda \right) = \exp \left(\int \frac{R\lambda^2 - (1 - \lambda)^2}{2\lambda(1 - \lambda)((R - 1)\lambda + 1)} d\lambda \right) = \exp \left(\int \frac{(R - 1)\lambda^2 + 2\lambda - 1}{2\lambda(1 - \lambda)((R - 1)\lambda + 1)} d\lambda \right) \\ &= \exp \left(\int \frac{(R - 1)\lambda(1 - \lambda) + ((R - 1)\lambda + 1)(2\lambda - 1)}{2\lambda(1 - \lambda)((R - 1)\lambda + 1)} d\lambda \right) = \exp \left(\int \frac{1}{2} \left(\frac{R - 1}{(R - 1)\lambda + 1} - \frac{1}{\lambda} + \frac{1}{1 - \lambda} \right) d\lambda \right) \\ &= \exp \left(\frac{1}{2} (\log|(R - 1)\lambda + 1| - \log|\lambda| - \log|1 - \lambda|) \right) = \sqrt{\frac{|(R - 1)\lambda + 1|}{\lambda(1 - \lambda)}}. \end{aligned}$$

This leads to

$$\frac{d}{dt} (v(\lambda)I(\lambda)) = 0 \iff v(\lambda)I(\lambda) = c_1.$$

Since $\dot{\lambda} = v(\lambda)$, the above is a separable first-order differential equation

$$\begin{aligned} \frac{d\lambda}{dt} I(\lambda) = c_1 &\iff \int I(\lambda) d\lambda = \int c_1 dt \\ \int \sqrt{\frac{|(R-1)\lambda+1|}{\lambda(1-\lambda)}} d\lambda &= c_1 t + c_2 \end{aligned}$$

For arbitrary $R > 0$, the above integral does not appear to have a closed-form solution. Crucially, however, when $R = 1$, i.e. if we choose $\sigma^2 = \mathbb{E}_\pi [\|X\|^2]/d$, then we have

$$c_1 t + c_2 = \int \sqrt{\frac{1}{\lambda(1-\lambda)}} d\lambda = \arcsin(2\lambda - 1).$$

The boundary conditions, $\lambda_0 = 0$ and $\lambda_1 = 1$, yield $c_2 = -\pi/2$ and $c_1 1 + c_2 = \pi/2$, respectively, so $c_1 = \pi$ and we arrive at the solution

$$\lambda_t = \frac{1 + \sin(\pi t - \frac{\pi}{2})}{2} = \frac{1 + \cos(\pi t)}{2} = \sin^2\left(\frac{\pi t}{2}\right).$$

To conclude, we show that the functional $J[\lambda]$ is convex, which should imply the stationary point we found is indeed a global minimiser. We check below that for any $\lambda_1, \lambda_2 \in C^1[0, 1]$ and any $\alpha \in [0, 1]$, it holds

$$J[\alpha\lambda_1 + (1-\alpha)\lambda_2] \leq \alpha J[\lambda_1] + (1-\alpha)J[\lambda_2].$$

For simplicity, we remove the constants and work with

$$J[\lambda] = \int_0^1 \frac{\dot{\lambda}_t^2}{\lambda_t(1-\lambda_t)} dt.$$

Consider the multivariate function $L(\lambda, \dot{\lambda}) = \frac{\dot{\lambda}^2}{\lambda(1-\lambda)}$, where $\lambda \in [0, 1]$ and $\dot{\lambda} \in \mathbb{R}$. The Hessian of this function is given by

$$\nabla^2 L = 2 \begin{pmatrix} \dot{\lambda}^2 \frac{\lambda(1-\lambda)+(1-2\lambda)^2}{\lambda^3(1-\lambda)^3} & -\dot{\lambda} \frac{1-2\lambda}{\lambda^2(1-\lambda)^2} \\ -\dot{\lambda} \frac{1-2\lambda}{\lambda^2(1-\lambda)^2} & \frac{1}{\lambda(1-\lambda)} \end{pmatrix}.$$

It is immediate to check that the determinant is

$$\det \nabla^2 L = \frac{4\dot{\lambda}^2}{\lambda^3(1-\lambda)^3} \geq 0,$$

and $(\nabla^2 L)_{22} \geq 0$, therefore, $\nabla^2 L$ is positive semidefinite and hence $L(\lambda, \dot{\lambda})$ is jointly convex in $(\lambda, \dot{\lambda})$. Using Van Brunt [2003, Theorem 10.7.1] this leads to

$$\begin{aligned} J[\alpha\lambda_1 + (1-\alpha)\lambda_2] &= \int_0^1 L(\alpha\lambda_1 + (1-\alpha)\lambda_2, \alpha\dot{\lambda}_1 + (1-\alpha)\dot{\lambda}_2) dt \\ &\leq \int_0^1 \alpha L(\lambda_1, \dot{\lambda}_1) + (1-\alpha)L(\lambda_2, \dot{\lambda}_2) dt \\ &= \alpha J[\lambda_1] + (1-\alpha)J[\lambda_2], \end{aligned}$$

which concludes that $J[\lambda]$ is convex and hence $\lambda_t = \sin^2(\frac{\pi t}{2})$ is a minimiser. \square

In fact, we now have the following upper bound for the action

Corollary A.1. *Under the choice $\sigma^2 = \mathbb{E}_\pi [\|X\|^2]/d$ and the cosine schedule $\lambda_t = \sin^2(\frac{\pi t}{2})$, the action is bounded by*

$$\mathcal{A}(\mu) \leq \frac{\mathbb{E}_\pi [\|X\|^2] \pi^2}{4}.$$

D Theoretical Analysis

In this section, we provide detailed proofs of our theoretical results.

D.1 Score Estimation Error

As discussed in the main text, when $\lambda_k \approx 0$, then $\varrho_{t,X} \approx \pi$, providing little benefit compared to addressing the original problem directly. However, as observed by He et al. [2024], when using the DSI for score estimation, it is possible to rely on less accurate samples from $\varrho_{t,X}$ in the Wasserstein-2 sense for small t , while still keeping the overall mean squared error of the Monte Carlo estimator below a given threshold.

We further analyse this behaviour for the weighted estimator constructed using the weighted particle system $\{(w_k^i, y_k^i)\}_{i=1}^N$ at the iteration k

$$S_k^N(x) = \mathbb{E}_{Y \sim \varrho_{t_k/T,x}^N} \left[\phi_{t_k/T,x}^{\alpha_k^* \mathbf{I}}(Y) \right] = \sum_{i=1}^N w_k^i \phi_{t_k/T,x}^{\alpha_k^* \mathbf{I}}(y_k^i),$$

where

$$\phi_{t_k/T,x}^{\alpha_k^* \mathbf{I}}(y) = \alpha_k^* \frac{\sqrt{\lambda_k} y - x}{\sigma^2(1 - \lambda_k)} + (1 - \alpha_k^*) \frac{\nabla \log \pi(y)}{\sqrt{\lambda_k}}$$

is the control variate score expression. Note that we define $\alpha_k^* := \alpha_{t_k/T}^*$ and $\lambda_k := \lambda_{t_k/T}$ for brevity.

We restate Proposition 4, which provides an upper bound on the L^2 error of the weighted score estimator (12), and present its proof.

Proposition 4 (Score estimation error). *Suppose Assumption 1 holds. Let $\{X_k\}_{k=1}^K$ such that $\hat{\mu}_{t_k} = \mathcal{L}(X_k)$ for all $k = 1, \dots, K$. Consider the score estimator $S_k^N(X_k)$ defined in (12) using a weighted particle system $\{(w_k^i, \bar{Y}_k^i)\}_{i=1}^N$ such that $\mathbb{E}[W_2^2(\sum w_k^i \delta_{\bar{Y}_k^i}, \varrho_{t_k/T,X_k})] \leq \delta(k, N)^2$ for all $k \geq 0$, then we have*

$$\mathbb{E} [\|\nabla \log \hat{\mu}_{t_k}(X_k) - S_k^N(X_k)\|^2] \leq 2\delta(k, N)^2 \left((\alpha_k^*)^2 \frac{\lambda_k}{(1 - \lambda_k)^2} + (1 - \alpha_k^*)^2 \frac{L_\pi^2}{\lambda_k} \right).$$

Proof. We have that

$$\begin{aligned} \mathbb{E} [\|\nabla \log \hat{\mu}_{t_k}(X_k) - \hat{s}_k(X_k)\|^2] &\leq 2(\alpha_k^*)^2 \mathbb{E} \left[\left\| \nabla \log \hat{\mu}_{t_k}(X_k) - \mathbb{E}_{Y \sim \varrho_{t_k/T,x_k}^N} \left[\frac{\sqrt{\lambda_k} Y - X_k}{\sigma^2(1 - \lambda_k)} | w_k^{1:N}, \bar{Y}_k^{1:N} \right] \right\|^2 \right] \\ &\quad + 2(1 - \alpha_k^*)^2 \mathbb{E} \left[\left\| \nabla \log \hat{\mu}_{t_k}(X_k) - \mathbb{E}_{Y \sim \varrho_{t_k/T,x_k}^N} \left[\frac{\nabla \log \pi(Y)}{\sqrt{\lambda_k}} | w_k^{1:N}, \bar{Y}_k^{1:N} \right] \right\|^2 \right] \\ &= 2(\alpha_k^*)^2 A + 2(1 - \alpha_k^*)^2 B \end{aligned}$$

Let η_{k,X_k} be any coupling between $\varrho_{t_k/T,X_k}^N$ and $\varrho_{t_k/T,X_k}$. We have the following bound for A

$$\begin{aligned} A &= \mathbb{E} \left[\left\| \mathbb{E}_{U \sim \varrho_{t_k/T,x_k}} \left[\frac{\sqrt{\lambda_k} U - X_k}{\sigma^2(1 - \lambda_k)} \right] - \mathbb{E}_{Y \sim \varrho_{t_k/T,x_k}^N} \left[\frac{\sqrt{\lambda_k} Y - X_k}{\sigma^2(1 - \lambda_k)} | w_k^{1:N}, \bar{Y}_k^{1:N} \right] \right\|^2 \right] \\ &= \frac{\lambda_k}{\sigma^4(1 - \lambda_k)^2} \mathbb{E} \left[\left\| \mathbb{E}_{U \sim \varrho_{t_k/T,x_k}, Y \sim \varrho_{t_k/T,x_k}^N} [U - Y | w_k^{1:N}, \bar{Y}_k^{1:N}] \right\|^2 \right] \\ &\leq \frac{\lambda_k}{\sigma^4(1 - \lambda_k)^2} \mathbb{E} \left[\mathbb{E}_{\eta_{k,X_k}} [\|U - Y\|^2 | w_k^{1:N}, \bar{Y}_k^{1:N}] \right]. \end{aligned}$$

Similarly, using that $\nabla \log \pi$ is Lipschitz continuous, we have

$$\begin{aligned} B &= \frac{1}{\lambda_k} \mathbb{E} \left[\left\| \mathbb{E}_{U \sim \varrho_{t_k/T,x_k}, Y \sim \varrho_{t_k/T,x_k}^N} [\nabla \log \pi(U) - \nabla \log \pi(Y)] \right\|^2 \right] \\ &\leq \frac{L_\pi^2}{\lambda_k} \mathbb{E} \left[\mathbb{E}_{\eta_{k,X_k}} [\|U - Y\|^2 | w_k^{1:N}, \bar{Y}_k^{1:N}] \right]. \end{aligned}$$

Combining the two bounds yields

$$\|\nabla \log \hat{\mu}_{t_k}(X_k) - \hat{s}_k(X_k)\|^2 \leq 2 \left((\alpha_k^*)^2 \frac{\lambda_k}{\sigma^4(1-\lambda_k)^2} + (1-\alpha_k^*)^2 \frac{L_\pi^2}{\lambda_k} \right) \mathbb{E}_{\eta_{t_k, X_k}} \left[\|U - Y\|^2 | w_k^{1:N}, \bar{Y}_k^{1:N} \right].$$

Taking the infimum over all couplings η , we obtain

$$\|\nabla \log \hat{\mu}_{t_k}(X_k) - \hat{s}_k(X_k)\|^2 \leq 2 \left((\alpha_k^*)^2 \frac{\lambda_k}{\sigma^4(1-\lambda_k)^2} + (1-\alpha_k^*)^2 \frac{L_\pi^2}{\lambda_k} \right) W_2^2 \left(\varrho_{t_k/T, X_k}, \varrho_{t_k/T, X_k}^N \right).$$

Finally, taking expectations and using the assumption, it follows

$$\mathbb{E} \left[\|\nabla \log \hat{\mu}_{t_k}(X_k) - \hat{s}_k(X_k)\|^2 \right] \leq 2 \delta(k, N^2) \left((\alpha_k^*)^2 \frac{\lambda_k}{\sigma^4(1-\lambda_k)^2} + (1-\alpha_k^*)^2 \frac{L_\pi^2}{\lambda_k} \right).$$

□

Due to the choice of α_t^* , our estimator exhibits similar behaviour to that of He et al. [2024] as $t \rightarrow 0$. In contrast, the setting considered in He et al. [2024] (which corresponds to taking $\alpha_t^* = 1$) requires an arbitrarily large number of samples as the algorithm approaches the target distribution ($t \rightarrow 1$) to maintain the L^2 bounded below some threshold. In our setting, however, as $t \rightarrow 1$, we can take $\alpha_t^* \approx 1 - \lambda_t$, implying that in the last expression above the term inside the parenthesis is of order $\mathcal{O}(1)$. This observation is consistent with the fact that DSI suffers from high variance in low-noise regimes.

The bound in Proposition 4 informs the choice of the number of particles N and the function $\delta(t, N)$ so that

$$\sum_{k=0}^{K-1} h \mathbb{E} \left[\|\nabla \log \hat{\mu}_{t_k}(X_k) - \hat{s}_k(X_k)\|^2 \right] \leq \varepsilon_{\text{score}}^2.$$

Therefore, we can apply the results of Cordero-Encinar et al. [2025a] to bound the final error of the algorithm. In particular, Theorem 1 provides an explicit result by particularising Theorem 3.4 in Cordero-Encinar et al. [2025a] to our setting.

E DPSMC Implementation

In this section, we briefly outline how DPSMC is implemented in practice. Our base algorithm in Algorithm 1 is presented as a generic, idealised version with non-interacting particles. However, as we do not know certain quantities, such as the target score covariance and the right step size for auxiliary variables, we estimate them using our ensemble of samples and auxiliary variables. Algorithm 2 depicts the scheme we use in practice.

Below we talk about the specific details of our sampler choices.

MALA proposal. Note that K_k^{MALA} is ρ_k -invariant, and under a suitable backwards kernel choice L_{k-1} as in (14), we have a simplified weight update given by the potential

$$G_k(y_{k-1}, y_k) = \frac{\tilde{\varrho}_{t_k/T, x_k}(y_{k-1})}{\tilde{\varrho}_{t_{k-1}/T, x_{k-1}}(y_{k-1})} = \frac{\mathcal{N}(\sqrt{\lambda_{t_k/T}} y_{k-1}; x_k, \sigma^2(1 - \lambda_{t_k/T}) \mathbf{I})}{\mathcal{N}(\sqrt{\lambda_{t_{k-1}/T}} y_{k-1}; x_{k-1}, \sigma^2(1 - \lambda_{t_{k-1}/T}) \mathbf{I})}.$$

For MALA, we scale the step size geometrically (i.e. by a factor of 1.1) to maintain an acceptance ratio of 75%. We chose a slightly larger scaling factor than those used in other samplers as we only do a single MALA step per iteration. Recall also that we heuristically stop the SMC sampler when the MALA acceptance ratio goes below a certain threshold. We set this threshold at 10%. The MALA proposal is presented in Algorithm 3.

Score estimation. We chose to use the matrix CV schedule for score estimation. Algorithm 4 shows how one would estimate this schedule using our samples, including the scalar and diagonal CV schedules for completeness.

Algorithm 2 DPSMC (Interacting)

input standard deviation of base Gaussian σ , initial distribution for auxiliary variables q_0 , step size $h = T/K$, number of samples N_X , number of auxiliary variables N_Y

- 1: $X_0^i \sim \mathcal{N}(0, \sigma^2 \mathbf{I})$ for all $i \in [N_X]$
- 2: $Y_0^{i,j} \sim q_0(\cdot)$ for all $i \in [N_X], j \in [N_Y]$
- 3: $A_0^{i,j} = -V_\pi(Y_0^{i,j}) - \log q_0(Y_0^{i,j})$ for all $i \in [N_X], j \in [N_Y]$
- 4: $S_0^i = -X_0^i / \sigma^2$ for all $i \in [N_X]$
- 5: **for** $k = 1, \dots, K-1$ **do**
- 6: **for** $i = 1, \dots, N_X$ **do**
- 7: $X_k^i \sim \mathcal{N}(\cdot; X_{k-1}^i + hS_{k-1}^i, 2h\mathbf{I})$ {ALD step}
- 8: **for** $j = 1, \dots, N_Y$ **do**
- 9: $\bar{Y}_k^{i,j} \sim K_k^{\text{MALA}}(\cdot | Y_{k-1}^{i,j}, X_k^i)$ {MALA step, see Alg. 3}
- 10: $A_k^{i,j} = A_{k-1}^{i,j} - \frac{\|X_k^i - \sqrt{\lambda_{t_k/T}} Y_{k-1}^{i,j}\|^2}{\sigma^2(1-\lambda_{t_k/T})} + \frac{\|X_{k-1}^i - \sqrt{\lambda_{t_{k-1}/T}} Y_{k-1}^{i,j}\|^2}{\sigma^2(1-\lambda_{t_{k-1}/T})}$
- 11: **end for**
- 12: **end for**
- 13: $w_k^{i,j} = \frac{\exp(A_k^{i,j})}{\sum_{l=1}^{N_Y} \exp(A_k^{i,l})}$ for all $i \in [N_X], j \in [N_Y]$
- 14: $\mathbf{A}_k = \text{CVSE}(\{w_k^{i,j}\}, \{\bar{Y}_k^{i,j}\}, \{X_k^i\})$ {CV schedule estimation, see Alg. 4}
- 15: **for** $i = 1, \dots, N_X$ **do**
- 16: $S_k^i = \sum_{j=1}^{N_Y} w_k^{i,j} \phi_{t_k/T, X_k^i}(\bar{Y}_k^{i,j})$ {Score estimation}
- 17: **if** $\widehat{\text{ESS}}(\{w_k^{i,j}\}_{j=1}^{N_Y}) < N_Y/2$ **then**
- 18: $\{Y_k^{i,j}\}_{j=1}^{N_Y} \sim \sum_{l=1}^{N_Y} w_k^{i,l} \delta_{\bar{Y}_k^{i,l}}(\cdot)$ {Resampling}
- 19: $A_k^{i,j} = 0$ for all $j \in [N_Y]$
- 20: **else**
- 21: $Y_k^{i,j} = \bar{Y}_k^{i,j}$ for all $j \in [N_Y]$.
- 22: **end if**
- 23: **end for**
- 24: **end for**
- 25: **for** $i = 1, \dots, N_X$ **do**
- 26: $X_K^i \sim \mathcal{N}(\cdot; X_{K-1}^i + hS_{K-1}^i, 2h\mathbf{I})$ {Final ALD step}
- 27: **end for**

output $\{X_K^i\}$

Algorithm 3 MALA Kernel

input auxiliary variable Y_{k-1} , sample X_k , temperature β_k (= 1 by default), step size h_{k-1} (adjusted automatically)

- 1: $q_k(y' | y) := \mathcal{N}(y'; y + h_{k-1} \nabla \log \varrho_{t_k/T, X_k}(y), \frac{2h_{k-1}}{\beta_k} \mathbf{I})$
- 2: $\tilde{Y}_{k+1} \sim q_{k+1}(\cdot | Y_k)$
- 3: $\alpha = \min \left\{ 1, \frac{\tilde{\varrho}_{t_k/T, X_k}(\tilde{Y}_k)^{\beta_k} q_k(Y_{k-1} | \tilde{Y}_k)}{\tilde{\varrho}_{t_k/T, X_k}(Y_{k-1})^{\beta_k} q_k(\tilde{Y}_k | Y_{k-1})} \right\}$
- 4: $Y_k \sim \alpha \delta_{\tilde{Y}_k}(\cdot) + (1 - \alpha) \delta_{Y_{k-1}}(\cdot)$

output Y_k

Adaptive resampling. Throughout, we perform adaptive resampling. Specifically, we resample only when the effective sample size (ESS), defined by

$$\widehat{\text{ESS}}(\{w_k^i\}) = \frac{1}{\sum_{i=1}^N (w_k^i)^2},$$

drops below a predefined threshold, which is half the number of auxiliary variables in our case. We employ this together with stratified resampling, a low-variance alternative to multinomial resampling, to avoid pruning out variables with large weights, which is inevitable after many time steps.

Algorithm 4 CV Schedule Estimation

input weights $\{w_k^{i,j}\}$, auxiliary variables $\{Y_k^{i,j}\}$, and samples $\{X_k^i\}$

$$1: \hat{\mathcal{I}}_\pi = \frac{1}{N_x} \sum_{i=1}^{N_x} \sum_{j=1}^{N_y} w_k^{i,j} \nabla \log \pi(Y_k^{i,j}) \nabla \log \varrho_{t_k/T, X_k^i} (Y_k^{i,j})^\top$$

$$2: \alpha_k = \frac{(1-\lambda_{t_k/T})\text{Tr}(\hat{\mathcal{I}}_\pi)}{\lambda_{t_k/T}d/\sigma^2 + (1-\lambda_{t_k/T})\text{Tr}(\hat{\mathcal{I}}_\pi)}$$

$$3: \mathbf{a}_k = \text{diag} \left(\left\{ \frac{(1-\lambda_{t_k/T})(\hat{\mathcal{I}}_\pi)_{ii}}{\lambda_{t_k/T}d/\sigma^2 + (1-\lambda_{t_k/T})(\hat{\mathcal{I}}_\pi)_{ii}} \right\}_{i=1}^d \right)$$

$$4: \mathbf{A}_k = \hat{\mathcal{I}}_\pi \left(\frac{\lambda_{t_k/T}}{\sigma^2(1-\lambda_{t_k/T})} \mathbf{I} + \hat{\mathcal{I}}_\pi \right)^{-1}$$

output α_k , \mathbf{a}_k , \mathbf{A}_k

Tempering. In the tempering case, we alter our path from $\rho_k(\cdot) = \varrho_{t_k/T, x_k}(\cdot)$ to $\rho_k^\beta(\cdot) \propto \varrho_{t_k/T, x_k}(\cdot)^{\beta_{t_k/T}}$. Our modified scheme is presented in Algorithm 5. Notably, whenever we estimate the score, we reweight our importance weights to estimate the normal (not tempered) posterior in expectation. In our experiments, we choose $\beta_t = \max\{\lambda_t, 10^{-2}\}$. We motivate this choice by considering a Gaussian posterior density. For $p(x) = \mathcal{N}(x; m, \sigma^2 \mathbf{I})$, the tempered distribution $q(x) \propto p(x)^{\beta_t}$ is given by $q(x) = \mathcal{N}(x; m, \frac{\sigma^2}{\beta_t} \mathbf{I})$. The Wasserstein-2 distance is then $W_2(p, q)^2 = \sigma^2 d(1 - 1/\sqrt{\beta_t})^2$. Under $\beta_t = \lambda_t$, we have $W_2(p, q) = \mathcal{O}((1 - \sqrt{\lambda_t})/\sqrt{\lambda_t})$, which satisfies the $\mathcal{O}(1/\sqrt{\lambda_t})$ scaling permitted in Proposition 4. Note that for general targets, and hence posterior densities, it is not trivial to design a schedule that can maintain the appropriate W_2 scaling. We also set a lower bound $\beta_{\min} = 10^{-2}$, chosen empirically, to act as a preventative measure for excessive tempering which can cause our auxiliary variables to diverge.

F Numerical Experiments

F.1 Methods and Hyperparameters

We detail here the hyperparameters of the methods we examine. For a majority of them, we follow the settings and hyperparameter grids outlined in Grenioux et al. [2024] when evaluating on targets that were previously considered. This includes incorporating information about the target, by way of R and τ , to each sampler. We recall their definition as coming from the following assumption.

Assumption 2 (Log concavity outside a compact). *There exists $R > 0$ and $\tau > 0$ such that π is the convolution of μ and $\mathcal{N}(0, \tau^2 \mathbf{I})$, where μ is a distribution compactly supported on $B = B(\mathbb{E}_\pi[X], R\sqrt{d})$, i.e. $\mu(\mathbb{R}^d \setminus B) = 0$.*

As our specific instantiation of GMM40 does not appear in Grenioux et al. [2024] and may be different from other setups, we test every combination of hyperparameters in the defined grid of each sampler and take the best result. Unless otherwise specified, samplers with MALA kernels use an adaptive step size that is geometrically adjusted to maintain an acceptance ratio of 75%. Additionally, we set the following parameters fixed globally across all samplers (except RDMC and the finer discretisation version of DPSMC, see individual discussions below) and benchmark targets

- Number of discretisation steps: $K = 1024$.
- Maximum number of energy evaluations (per sample): $N_{\text{evals}} = 1.32 \times 10^5$.

AIS and SMC. Both AIS and SMC operate on the geometric path, i.e. $\rho_k(x) \propto \rho_0(x)^{1-\beta_k} \pi(x)^{\beta_k}$ for $k \in \{1, \dots, K\}$, where we have a Gaussian initial density $\rho_0(x) := \mathcal{N}(0, (R^2 d + \tau^2) \mathbf{I})$ and a linear annealing schedule $\beta_k = k/K$. Transitions between the path marginals are made via MALA transition kernels. Specifically, each sample runs 128 MALA steps per iteration. In SMC, the samples are adaptively resampled according to their importance weights whenever the ESS drops below half the number of particles. We find this performs better than the original settings in Grenioux et al. [2024] where they use fewer MALA steps and resample at every time step.

Algorithm 5 DPSMC (Interacting) with Tempered Auxiliary Distributions

input standard deviation of base Gaussian σ , initial distribution for auxiliary variables q_0 , step size $h = T/K$, inverse temperature schedule β_t , number of samples N_X , number of auxiliary variables N_Y

- 1: $X_0^i \sim \mathcal{N}(0, \sigma^2 \mathbf{I})$ for all $i \in [N_X]$
- 2: $Y_0^{i,j} \sim q_0(\cdot)$ for all $i \in [N_X], j \in [N_Y]$
- 3: $A_0^{i,j} = -\beta_0 V_\pi(Y_0^{i,j}) - \log q_0(Y_0^{i,j})$ for all $i \in [N_X], j \in [N_Y]$
- 4: $S_0^i = -X_0^i / \sigma^2$ for all $i \in [N_X]$
- 5: **for** $k = 1, \dots, K-1$ **do**
- 6: **for** $i = 1, \dots, N_X$ **do**
- 7: $X_k^i \sim \mathcal{N}(\cdot; X_{k-1}^i + hS_{k-1}^i, 2h\mathbf{I})$ {ALD step}
- 8: **for** $j = 1, \dots, N_Y$ **do**
- 9: $\bar{Y}_k^{i,j} \sim \mathsf{K}_k^{\text{MALA}}(\cdot | Y_{k-1}^{i,j}, X_k^i, \beta_{t_k/T})$ {MALA step, see Alg. 3}
- 10: $A_k^{i,j} = A_{k-1}^{i,j} + \beta_{t_{k+1}/T} \log \tilde{\varrho}_{k+1, X_{k+1}^i}(Y_k^{i,j}) - \beta_{t_k/T} \log \tilde{\varrho}_{k, X_k^i}(Y_k^{i,j})$
- 11: **end for**
- 12: **end for**
- 13: $\tilde{w}_k^{i,j} = \frac{\exp(A_k^{i,j} + (1 - \beta_{t_k/T}) \log \tilde{\varrho}_{t_k/T, X_k^i}(Y_k^{i,j}))}{\sum_{l=1}^N \exp(A_k^{i,l} + (1 - \beta_{t_k/T}) \log \tilde{\varrho}_{t_k/T, X_k^i}(Y_k^{i,l}))}$ for all $i \in [N_X], j \in [N_Y]$ {Corrected importance weights}
- 14: $w_k^{i,j} = \frac{\exp(A_k^{i,j})}{\sum_{l=1}^{N_Y} \exp(A_k^{i,l})}$ for all $i \in [N_X], j \in [N_Y]$
- 15: **A_k** = CVSE($\{\tilde{w}_k^{i,j}\}, \{\bar{Y}_k^{i,j}\}, \{X_k^i\}$) {CV schedule estimation, see Alg. 4}
- 16: **for** $i = 1, \dots, N_X$ **do**
- 17: $S_k^i = \sum_{j=1}^{N_Y} \tilde{w}_k^{i,j} \phi_{t_k/T, X_k^i}^{\mathbf{A}_k}(\bar{Y}_k^{i,j})$ {Score estimation}
- 18: **if** $\widehat{\text{ESS}}(\{w_k^{i,j}\}_{j=1}^{N_Y}) < N_Y/2$ **then**
- 19: $\{Y_k^{i,j}\}_{j=1}^{N_Y} \sim \sum_{l=1}^{N_Y} w_k^{i,l} \delta_{\bar{Y}_k^{i,l}}(\cdot)$ {Resampling}
- 20: $A_k^{i,j} = 0$ for all $j \in [N_Y]$
- 21: **end if**
- 22: **end for**
- 23: **end for**
- 24: **for** $i = 1, \dots, N_X$ **do**
- 25: $X_K^i \sim \mathcal{N}(\cdot; X_{K-1}^i + hS_{K-1}^i, 2h\mathbf{I})$ {Final ALD step}
- 26: **end for**

output $\{X_K^i\}$

RDMC. Here, the final time T in the OU process is treated as a hyperparameter. Following Huang et al. [2024], we search for its values in the grid $\{-\log(0.99), -\log(0.95), -\log(0.9), -\log(0.8), -\log(0.7)\}$. We explain briefly how RDMC is implemented. To start, samples are drawn from $\mathcal{N}(0, (1 - e^{-2T})\mathbf{I})$ and 16 iterations of the Langevin-within-Langevin procedure are performed. Here, and at every iteration afterwards, 128 samples are drawn from the Gaussian component of the posterior to form an IS estimate of the posterior mean. This serves as the initialisation of four chains that run 32 MALA steps, the first half of which are considered part of a warm-up and discarded. All combined, the 64 samples (auxiliary variables) are used to estimate the posterior mean and hence the score. Note that this totals to $(16 + 1024) \times (128 + 4 \times 32) = 2.66 \times 10^5$ energy evaluations. While this is more than the imposed budget, we stick to this formulation so we can choose the optimal hyperparameters from Grenioux et al. [2024] for benchmarks other than GMM40. Its chosen settings across benchmarks are listed in Table 2.

	GMM40 ($d = 2$)	GMM ($d = 50$)	Rings	Funnel	Ionosphere	Sonar
End Time (T)	$-\log(0.70)$	$-\log(0.80)$	$-\log(0.80)$	$-\log(0.90)$	$-\log(0.95)$	$-\log(0.95)$

Table 2: Chosen values for the end time T for RDMC across the several benchmark targets.

SLIPS. We use the classic variant of SLIPS in our experiments. Similar to RDMC, it undergoes a Langevin-within-Langevin initialisation for the same number of iterations and estimates the posterior mean using four chains taking 32 MALA steps, half being warm-up steps. However, instead of using IS estimates to initialise the chains, it uses the positions of the chains in the previous time step. Furthermore, SLIPS starts at some later time t_0 for which both the path marginals and posterior distribution are assumed to be approximately log-concave. For GMM40, we perform a search along the grids $\eta = \{5.0, 5.7\}$ and $t_0 = \{0.1, 0.2, 0.4, 1.0, 1.2\}$, similar to the grid search suggested for mixtures in Grenioux et al. [2024]. Its chosen settings across benchmarks are listed in Table 3.

	GMM40 ($d = 2$)	GMM ($d = 50$)	Rings	Funnel	Ionosphere	Sonar
Log SNR Threshold (η)	5.0	5.7	4.6	5.0	5.0	5.0
Start Time (t_0)	1.20	0.10	1.20	1.00	0.03	0.03

Table 3: Chosen values for the log SNR threshold η and start time t_0 for SLIPS across the several benchmark targets.

DPSMC. We run annealed Langevin dynamics for $t \in [0, T]$ using $\sigma^2 = \mathbb{E}_\pi[\|X\|^2]/d$ and the cosine schedule $\lambda_t = \sin^2(\frac{\pi t}{2})$ in all our experiments. We choose T as follows. Corollary A.1 indicates the following upper bound on the action

$$\mathcal{A}(\mu) \leq \int_0^1 \left(\frac{\sigma^2 d}{4(1 - \lambda_t)} + \frac{\mathbb{E}_\pi[\|X\|^2]}{4\lambda_t} \right) (\partial_t \lambda_t)^2 dt = \frac{\mathbb{E}_\pi[\|X\|^2]\pi^2}{4},$$

which is achieved precisely under our choices of base Gaussian variance and cosine schedule. Now, using this result in the workings of Theorem 3.4 of [Cordero-Encinar et al., 2025a], we can write

$$\text{KL}(\mathbb{P} \parallel \mathbb{Q}) \lesssim \left(1 + \frac{L^2 T^4}{K^2}\right) \frac{\mathbb{E}_\pi[\|X\|^2]\pi^2}{4T} + \frac{dL^2 T^2}{K} \left(1 + \frac{LT}{K}\right) + \varepsilon_{\text{score}}^2,$$

where \mathbb{P} is the reference path measure, \mathbb{Q} is the path measure of the continuous-interpolation of diffusion annealed Langevin Monte Carlo, L is the supremum of the Lipschitz constants of $\nabla \log \mu_t$ along the path, and $\varepsilon_{\text{score}}^2$ is the score error. Loosely, we choose T such that it minimises the first two terms. Taking the derivative with respect to T and setting to zero, we have

$$\frac{\mathbb{E}_\pi[\|X\|^2]\pi^2}{4} \left(-\frac{1}{T^2} + \frac{3L^2 T^2}{K^2} \right) + \frac{2dL^2 T}{K} + \frac{3dL^3 T^2}{K^2} = 0.$$

Assuming the $O(1/K^2)$ vanishes, e.g. for large enough K , we then have

$$-\frac{\mathbb{E}_\pi[\|X\|^2]\pi^2}{4T^2} + \frac{2dL^2T}{K} = 0 \iff T = \left(\frac{K\mathbb{E}_\pi[\|X\|^2]\pi^2}{8dL^2}\right)^{1/3}.$$

We use this crude approximation and set $T = \xi \left(\frac{K\mathbb{E}_\pi[\|X\|^2]}{d}\right)^{1/3}$, for some hyperparameter ξ which we find in the grid

$$\left\{2^{\left[-2.5 \cdot \left(1 - \frac{i}{10}\right) + 3.5 \cdot \frac{i}{10}\right]} \mid i \in \{0, \dots, 10\}\right\},$$

i.e. linearly interpolating in log-space. The chosen values in our experiments are given in Table 4. Along with the normal instantiation of DPSMC, we also test its version with a tempered posterior path and another where the discretisation was eight times finer but had fewer auxiliary variables. For tempering, we use the same hyperparameters as the normal instantiation. As for the finer discretisation, we generally expect to see ξ values that are approximately the same as in the normal scheme with fewer discretisation steps, given K is accounted for in our expression. This is true for most targets except Rings and Funnel, which shows a potential limitation of our crude approximation for T . We remark however that DPSMC had local minima at opposite ends of the grid for the Rings benchmark, regardless of the discretisation. It so happens that a different one was chosen for each discretisation.

	GMM40 ($d = 2$)	GMM ($d = 50$)	Rings	Funnel	Ionosphere	Sonar
ξ	$2^{3.5}$	$2^{2.9}$	$2^{-2.5}$	$2^{-0.1}$	$2^{-2.5}$	$2^{-2.5}$
ξ (8x)	$2^{3.5}$	$2^{2.9}$	$2^{2.3}$	$2^{0.5}$	$2^{-2.5}$	$2^{-2.5}$
Simulation Time (T)	584.25	387.66	2.77	15.33	1.88	1.84
Simulation Time (T) (8x)	1168.51	775.33	154.37	46.48	3.76	3.68

Table 4: Chosen hyperparameter values for DPSMC and the resulting T value across the several benchmark targets. Rows affixed with "(8x)" indicate the chosen values corresponding to the DPSMC 8x discretisation scheme. See Table 5 for the second moments of the targets used to compute T .

F.2 Target Distributions

We detail here the targets that were considered in our experiments. As we use the expected squared norm $\mathbb{E}_\pi[\|X\|^2]$ in our methods, we precisely write down their expressions or approximations if unavailable. A summary of their values are available in Table 5, including the choices for (R, τ) made by Grenioux et al. [2024] to be used for the other samplers.

GMM40. We consider a uniform mixture of 40 Gaussians in d dimensions with identity covariance matrices and means sampled uniformly from a d -dimensional hypercube of side length 40. The density is exactly given by

$$\pi(x) = \frac{1}{40} \sum_{i=1}^{40} \mathcal{N}(x; \mathbf{m}_i, \mathbf{I}),$$

for $\mathbf{m}_i \sim U[-20, 20]^d$. We therefore have the expected squared norm equal to

$$\mathbb{E}_\pi[\|X\|^2] = d + \frac{1}{40} \sum_{i=1}^{40} \|\mathbf{m}_i\|^2.$$

We then appropriately set $R = \frac{1}{\sqrt{d}} \max_{i \in [d]} \{\|\mathbf{m}_i - \frac{1}{40} \sum_{j=1}^{40} \mathbf{m}_i\|^2\}$ and $\tau = 1$. In our experiments, we fix the seed (0) when sampling the mean vectors. Under these choices, we arrive at values shown in Table 5.

Rings. The rings distribution [Grenioux et al., 2024] is a radially symmetric distribution featuring four concentric rings of different radii as the regions with high density. First, we define two univariate distributions: a radial one p_r given by

$$p_r(x) = \frac{1}{4} \sum_{i=1}^4 \mathcal{N}(x; i, 0.15^2),$$

and an angular one p_θ that is a uniform distribution over $[0, 2\pi]$. The rings distribution is precisely the inverse polar reparameterisation of the joint distribution of both radial and angular components, i.e.

$$\pi(x) = p_r(\|x\|)p_\theta(\tan^{-1}(x_1/x_2)).$$

Given the rotational symmetry, it suffices to look at the radial component to compute the expected squared norm. We have

$$\mathbb{E}_\pi[\|X\|^2] = \mathbb{E}_{p_r}[X^2] = \frac{1}{4} \sum_{i=1}^4 (i^2 + 0.15^2) = 7.5225.$$

Funnel. The funnel distribution [Neal, 2003] is a hierarchical distribution featuring an exponentially narrowing region of high density. It is exactly given by

$$\pi(x) = \mathcal{N}(x_1; 0, \eta^2) \prod_{i=2}^{10} \mathcal{N}(x_i; 0, \exp(x_1)\mathbf{I}),$$

for some η^2 . While Grenioux et al. [2024] claim to use $\eta = 3$, we found their code to have actually used $\eta^2 = 3$ when assessing their sampler and its hyperparameters. We accordingly use $\eta^2 = 3$ for our experiments. We now solve for its expected squared norm. We have that

$$\begin{aligned} \mathbb{E}_\pi[\|X\|^2] &= \eta^2 + \int \frac{1}{\sqrt{2\pi\eta^2}} \exp\left(-\frac{x_1^2}{2\eta^2}\right) \int \frac{1}{\sqrt{2\pi \exp(x_1)}} \exp\left(-\frac{\|x_{2:10}\|^2}{2\exp(x_1)}\right) \|x_{2:10}\|^2 dx_{2:10} dx_1 \\ &= \eta^2 + \int \frac{1}{\sqrt{2\pi\eta^2}} \exp\left(-\frac{x_1^2}{2\eta^2}\right) (9\exp(x_1)) dx_1 \\ &= \eta^2 + 9\exp(\eta^2/2) \approx 43.34 \end{aligned}$$

where we used the fact that the MGF for a univariate gaussian $p(x) = \mathcal{N}(x; \mu, \sigma^2)$ is $\mathbb{E}_p[\exp(tX)] = \exp(\mu t + t^2\sigma^2/2)$.

Bayesian logistic regression. Given a dataset $\mathcal{D} = \{(x_i, y_i)\}_{i=1}^M$ with vector-valued features $x_i \in \mathbb{R}^d$ and binary outcomes $y_i \in \{0, 1\}$ for $i \in [M]$, a Bayesian logistic regression model is given by a prior on its weight vector $w \in \mathbb{R}^d$ and intercept $b \in \mathbb{R}$ which we choose to be

$$p(w, b) = \mathcal{N}(w; 0, \mathbf{I})\mathcal{N}(b; 0, 2.5^2),$$

and a likelihood for a pair (x, y) in terms of the model parameters

$$p(y | x; w, b) = \text{Bernoulli}(y; \sigma(w^\top x + b)),$$

where $\sigma(x) = \frac{\exp(x)}{1+\exp(x)}$ is the sigmoid function. The goal is to sample from the posterior distribution

$$\pi(w, b) := p(w, b | \mathcal{D}) \propto p(\mathcal{D} | w, b)p(w, b) = \left[\prod_{i=1}^M p(y_i | x_i; w, b) \right] p(w, b).$$

Instead of computing the expected squared norm of the model parameters with respect to the posterior, we compute our statistics based on the prior directly, i.e. we have

$$\mathbb{E}_p[\|W\|^2 + B^2] = d \cdot 1 + 2.5^2 = d + 6.25.$$

Target	$\mathbb{E}_\pi[\ X\ ^2]$	σ	R	τ
GMM40 ($d = 2$)	268.98	11.60	18.33	1
GMM40 ($d = 50$)	6840.25	11.70	67.10	1
Rings ($d = 2$)	7.52	1.94	$4/\sqrt{2}$	0.15
Funnel ($d = 10$)	43.34	2.08	2.12	0
Ionosphere ($d = 35$)	≈ 41.25	1.09	$2.5/\sqrt{36}$	0
Sonar ($d = 61$)	≈ 67.25	1.05	$2.5/\sqrt{62}$	0

Table 5: The specific values of target information used to inform samplers across several target distributions.

G Additional Experiments

G.1 Sampling in the Absence of the Compact Set’s Radius

In our experiments, we informed all the samplers, including DPSMC, with the decomposition of the target as a convolution of a distribution supported on a compact ball with radius $R\sqrt{d}$ and a Gaussian with isotropic variance τ^2 . However, this can be rather restrictive. In its absence, we consider simply using the target’s second moment $\mathbb{E}_\pi[\|X\|^2]$, a quantity that is arguably more accessible, although less informative of the target. We initialise auxiliary variables according to $q_0(y) = \mathcal{N}(y; 0, \sigma^2 \mathbf{I})$, for $\sigma^2 = \mathbb{E}_\pi[\|X\|^2]/d$. We summarise our findings in Table 6.

Algorithm	Batched	GMM40 Evals (\downarrow) ($d = 2$)	GMM40 ($d = 50$)	Rings ($d = 2$)	Funnel ($d = 10$)	Ionosphere ($d = 35$)	Sonar ($d = 61$)
DPSMC	1K	2.05 ± 0.15	69.94 ± 0.51	0.21 ± 0.03	0.060 ± 0.004	-83.89 ± 0.13	-109.22 ± 0.06
DPSMC w/ Tempering	1K	1.75 ± 0.20	34.35 ± 1.42	0.22 ± 0.02	0.138 ± 0.006	-83.96 ± 0.11	-108.56 ± 0.07

Table 6: Performance of DPSMC in the absence of R and τ , i.e. only using $\mathbb{E}_\pi[\|X\|^2]$. The performance across most problems are kept largely the same except GMM40, where poor coverage of modes at initialisation can impact performance. Notably, tempering allows better mode exploration.

G.2 Comparison with Parallel Tempering

Parallel tempering (PT) [Swendsen and Wang, 1986, Geyer and Thompson, 1995] has largely remained as the gold standard amongst sampling methods. It defines a sequence of inverse temperatures $0 < \beta_1 < \dots < \beta_{N_B} = 1$ and subsequently targets the joint distribution $p(x_1, \dots, x_{N_B}) \propto \prod_{i=1}^{N_B} \pi(x_i)^{\beta_i}$. To do this, it runs several Markov chains in parallel, one at each temperature level, often via Hamiltonian Monte Carlo (HMC) [Neal et al., 2011] samplers. After every step, chains at different temperature levels, e.g. adjacent ones, are swapped according to some probability that leaves the joint distribution invariant. This scheme allows the chain at the normal temperature to traverse between modes through swaps with chains at higher temperatures where the energy barriers present are significantly lower.

We chose not to include PT in our main table as it is fundamentally different in its equilibrium nature. However, we thought it was important to show its performance as a standard reference. We report our findings in Table 7. Below we describe our choices for its settings.

Batched	GMM40	GMM40	Rings	Funnel	Ionosphere	Sonar
Evals (\downarrow)	($d = 2$)	($d = 50$)	($d = 2$)	($d = 10$)	($d = 35$)	($d = 61$)
2M	1.13 ± 0.18	42.44 ± 2.13	0.18 ± 0.02	0.022 ± 0.005	-87.91 ± 0.17	-111.04 ± 0.08

Table 7: Performance of parallel tempering on the benchmark problems. Results highlighted in **bold** indicate it achieved the best performance amongst the samplers we tested.

We fix the number of chains to be $N_B = 16$ and set the inverse temperatures to be $\beta_i = 10^{-(i-1)/5}$. While we would normally run a single instance of PT and take the positions of the coldest chain at every number of steps, we chose to run 16 parallel instances else runtimes became unreasonably long. Each chain runs an HMC sampler. Simulating Hamiltonian dynamics requires specifying the mass matrix M , the step size h , and the number of leapfrog steps L . We set the mass matrix to be the identity $M = \mathbf{I}$ and choose a step size h that achieves roughly 0.65 acceptance ratio [Neal et al., 2011]. First, we initialise 64 chains per temperature level from $\mathcal{N}(0, (R^2 d + \tau^2) \mathbf{I})$ and do 200 warm-up steps to geometrically adjust the step size (per temperature) to achieve the target acceptance ratio. Then, we only keep 16 samples (number of instances) at each temperature level, and, for every subsequent HMC step, we use the same step size obtained after the warm-up. We choose the number of leapfrog steps L to be equal to 128, and we take the coldest chain's position after every 64 HMC steps and treat them as our samples. To be precise, the total energy evaluations (which should be less than $N_{\text{evals}} \times 4096$) is the product the following quantities: number of instances (16), number of chains/temperatures (16), number of HMC steps (64), number of leapfrog steps (128), number of samples per instance (256).